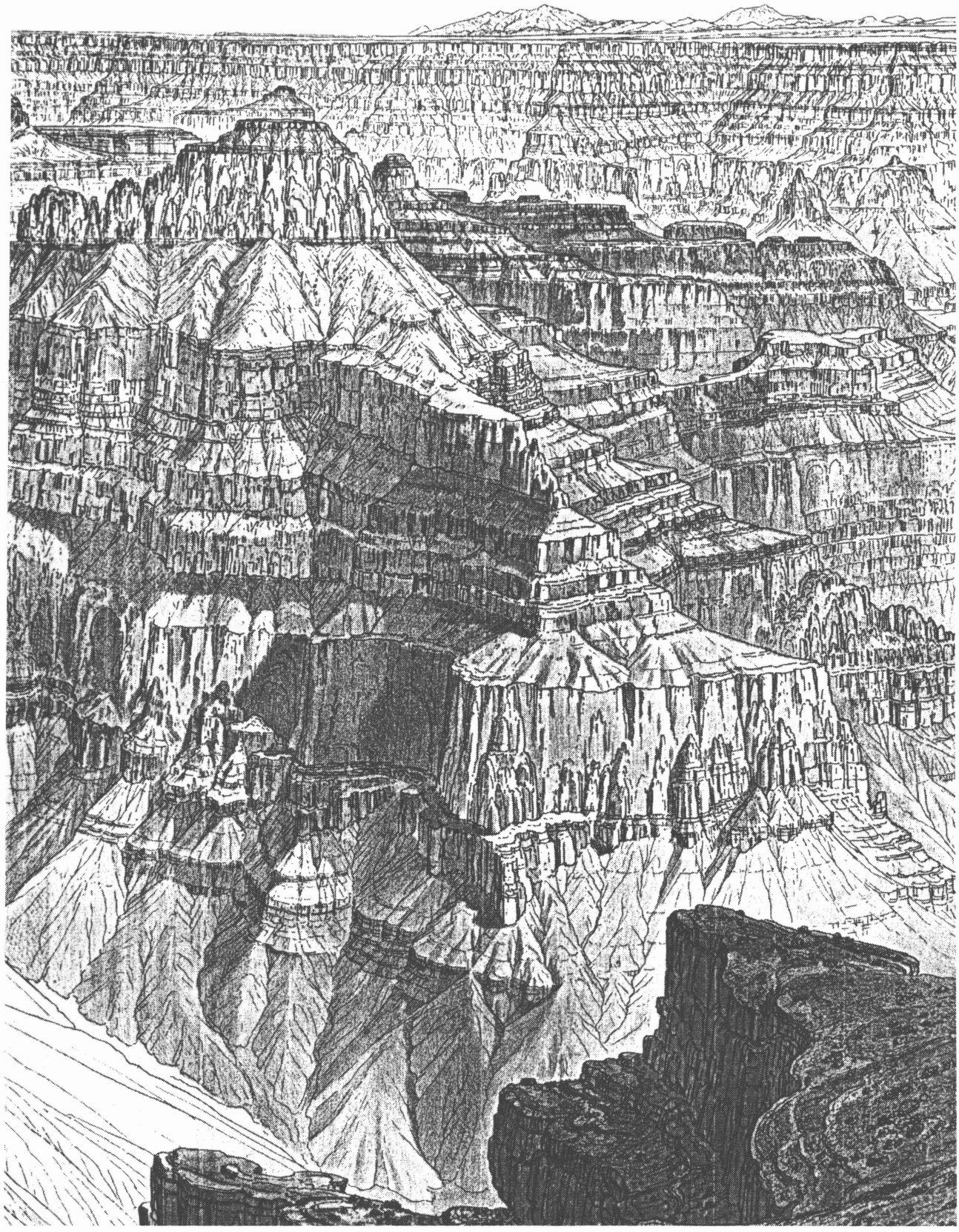

Frontispiece: Panorama from Point Sublime in the Kaibab, north rim of the Grand Canyon, drawn by William H. Holmes. Note the stratabound nature of fractures in the units of the Grand Canyon section. Figure source is sheet XV, USGS atlas to accompany the Tertiary history of the Grand Canyon district, by Clarence E. Dutton, 1882.

Physical and Hydrologic-Flow Properties of Fractures

Las Vegas, Nevada - Zion Canyon, Utah - Grand Canyon, Arizona - Yucca Mountain, Nevada
July 20–24, 1989

Field Trip Guidebook T385

Leaders:
Christopher C. Barton and Paul A. Hsieh

Associate Leaders:
Jacques Angelier, Francoise Bergerat, Catherine Bouroz, Michael D. Dettinger, and Edwin P. Weeks

Published 1989 by American Geophysical Union

2000 Florida Ave., N.W., Washington, D.C. 20009

ISBN: 0-87590-650-8

Printed in the United States of America

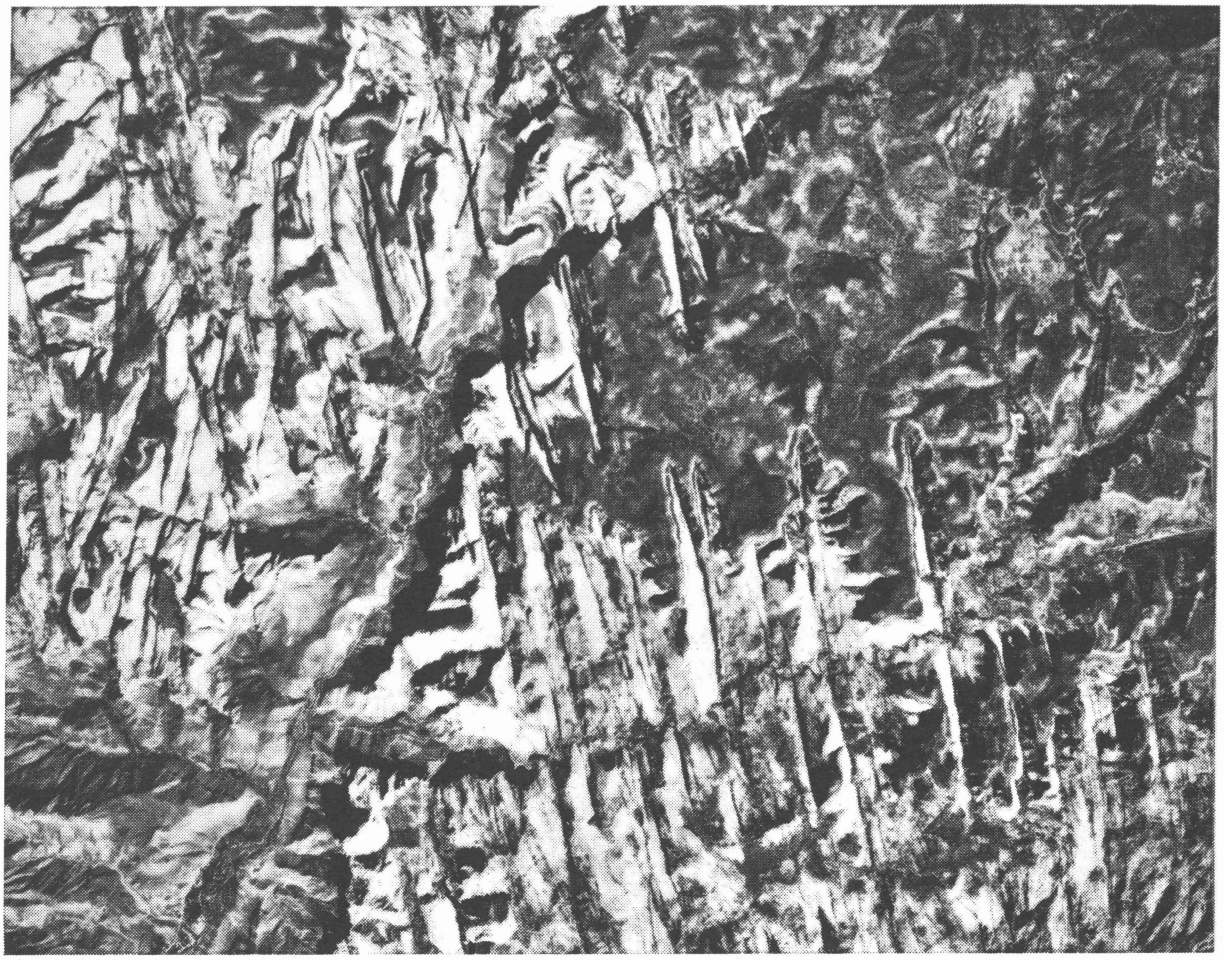

Cover Photo: Aerial view of megascopic fracture pattern in the Navajo sandstone at Zion National Park. The town of Springdale, Utah and Zion Canyon extend to the NNE from the bottom left of the photo. The prominent fracture set strikes approximately N11W throughout the region. A second set, visible to the west of Zion Canyon, strikes approximately N13E. Scale is 1:57,000. Photo source number NHAP 84, 148-7, courtesy of the U.S. Geological Survey.

Leaders:

Christopher C. Barton
U.S. Geological Survey
Federal Center, MS 913
Denver, CO 80225

Paul A. Hsieh
U.S. Geological Survey
345 Middlefield Road, MS 496
Menlo Park, CA 94025

Associate Leaders:

Jacques Angelier, Francoise Bergerat, and Catherine Bouroz
Universite Pierre et Marie Curie
Departement de Geotectonique, T26-25-E1
Laboratoire de Geologie Structurale
4 Place Jussieu
75252 Paris Cedex 05
France

Michael D. Dettinger
U.S. Geological Survey
705 North Plaza
Carson City, NV 89701

Edwin P. Weeks
U.S. Geological Survey
Federal Center, MS 413
Denver, CO 80225

TABLE OF CONTENTS

PART I - GENERAL BACKGROUND

PART II - DESCRIPTION OF STOPS

PART III - ROAD LOG

Physical and Hydrologic-Flow Properties of Fractures

IGC FIELD TRIP T385:
PHYSICAL AND HYDROLOGIC-FLOW PROPERTIES OF FRACTURES

Christopher C. Barton
U.S. Geological Survey, Denver, Colorado

Paul A. Hsieh
U.S. Geological Survey, Menlo Park, California

PART I - GENERAL BACKGROUND

INTRODUCTION

Fractures are one of the most abundant structures in geology and are found in almost all rocks and soils at or near the Earth's surface. They are found over a wide range of length scales, from micro-fractures within mineral grains (micro-meters) to oceanic-intraplate fractures as much as 5000 km in length. The important role of fractures in fluid transport in the crust has long been recognized by geologists who have studied dikes (fracture conduits for flow of igneous rocks) and mineral veins (fracture conduits for precipitation from aqueous fluids). In studying these paleo-flow systems, little attention has been given to quantification of the flow properties of the system. Until two decades ago, hydrologists (Long, 1983) and petroleum-reservoir engineers (Nelson, 1985) studying fluid flow in rock had recognized the role of fractures only qualitatively. Quantitatively, the mathematics of fracture flow had been considered intractable while the mathematics of porous-media flow through the rock matrix had been developed and refined for almost one hundred years. Direct observation of the flow properties of rock at field scales demonstrated the inadequacy of the porous media models beyond the scale of laboratory samples. The hydraulic conductivity of fractured bulk rock has been measured to be as much as 8 orders of magnitude greater than matrix hydraulic conductivity measured in laboratory samples of the same intact rock. Clearly, fractures are primary conduits for fluid flow in rock at time scales of economic and practical interest. Quantitative understanding of the physics of flow in individual fractures and fracture networks has become an important research topic with direct applications to contemporary and paleo flow systems.

In order to understand fracture flow, it is necessary to understand the physical parameters of the fractures that affect flow. These include orientation, roughness, aperture, size, shape, and mineral fillings for individual fractures, and density, connectivity, spatial distribution, and scaling laws for fracture networks.

On this field trip you will see some of the most spectacular physiography and geology in the southwestern United States as described briefly in the road log. However, the geologic setting and history are not the primary purpose of this trip. The purpose of this field guide and the trip is to introduce the reader to the significance of the fracture parameters listed above, to quantitative methods for measuring them in the field, and to the hydrology of fractured rock.

The route followed and the location of the field trip stops are shown in figure 1. Each stop is identified by two numbers separated by a dash. The first number is the day, and the second is the stop number. We suggest following the roadlog using the following regional geologic maps and cross section: Nevada (Stewart and Carlson, 1978), Utah (Hintze, 1980), Arizona (Wilson and others, 1969), and the geologic cross section of Cedar Breaks-Zion-Grand Canyon Region (Breed, 1975). Geologic maps at larger scales are referenced in the text for each stop.

In the past five years there have been several symposia on fractures and fracture flow. Three symposia that have published proceedings at the time of this writing are: Farmer and others, 1987; the 17th Congress of the International Association of Hydrogeologists, 1985; and Stephansson, 1985.

Acknowledgments

We are indebted to Dwight L. Schmidt, Edward G. Sable, Isaac J. Winograd, Michael D. Dettinger, and Geoffrey W. Freethey of the U.S. Geological Survey, to Jacques Angelier, Francoise Bergerat, and to Catherine Bouroz of the University of Paris, who have generously shared their knowledge of the geology, fractures, and hydrology of southeastern Nevada and the Zion and Grand Canyon regions.

GEOLOGIC SETTING

The trip will take place in parts of two tectonic and physiographic provinces, the Basin and Range Province and the Colorado Plateau. A brief summary of their geologic histories below is based on Hamilton (1987 and 1988).

This part of the Basin and Range Province is underlain by Triassic and Jurassic granitic intrusions and was affected by Jurassic metamorphism and deformation, voluminous Eocene, Oligocene, and early Miocene arc magmatism, and Paleocene volcanic and intrusive activity as evidenced by ignimbrite fields and small granitic plutons. Extension began in the area in early Oligocene and

continued through to the present, but has been irregular in time and space.

The Colorado Plateau is underlain by a crystalline basement of Proterozoic metamorphic, plutonic, and continental accretionary wedges, postdated by Middle to Late Proterozoic sedimentation, volcanism, and normal faulting, and was eroded regionally to a surface of low relief. This was followed by deposition of Upper Cambrian and lower Paleozoic clastic and carbonate platform sediments from the Cambrian Tapeats Sandstone through the Mississippian Redwall Limestone as exposed in the Grand Canyon section. In Middle Pennsylvanian time, moderate crustal shortening (possibly related to a South American-North American collision) produced broad thrust-bounded ranges and basins. The thick, bedded sequence of the Pennsylvanian and Lower Permian Supai Group of the Grand Canyon were deposited in the basins. The overlying Hermit Shale and Coconino Sandstone were derived from the remnants of these uplifts. The Upper Permian through Mesozoic sedimentary rocks of the Colorado Plateau were largely platformal, with variable contributions of volcanic ash from the west and clastic sediments derived from uplifts mostly to the west.

The Colorado Plateau has been left mostly unaffected by surrounding tectonism. It lacks the thin-skinned Sevier (Late Jurassic and possibly Cretaceous) deformation to the north and west, perhaps because it does not have the wedge of shearable sediments requisite for foreland thrusting. The plateau was deformed in the Pennsylvanian as discussed above. The Laramide deformation (latest Cretaceous through Eocene) resulted in slight crustal shortening and the formation of major monoclinal structures and approximately 4° of clockwise rotation of the plateau. The plateau has been only slightly affected by Neogene Basin and Range extension and by approximately 2° of clockwise rotation from late Oligocene to early Miocene; it was not affected by middle Tertiary magmatism, which was extensive farther east and to the west. Uplift of the Colorado Plateau from middle Miocene time to the present is part of the laterally extensive Rocky Mountain, Great Plains, and Great Basin uplift and has permitted the erosional incision which has produced the spectacular canyons.

The approximate boundary between the Basin and Range Province and the Colorado Plateau in the area of the field trip (fig. 1) is the Paleozoic hinge line between the cratonic platform to the east and the continental shelf to the west.

FRACTURE TERMINOLOGY

Because fractures have been studied extensively in rock, soil, metals, glass, ceramics, and other materials, there is an abundant overlapping, conflicting, and sometimes vague terminology in the geologic literature. Some of the existing terms are defined in terms of--or hold connotations about--the mode of fracture origin. We have reduced the varied terminology to a minimum of three hierarchical terms that do not incorporate any assumptions about mode of origin and are based solely on the relative sense of offset across the opposing faces, a single characteristic that can be distinguished by direct observation.

A FRACTURE is a planar or curvi-planar parting across which coherence has been lost. Fractures are distinguished from and do not include the other surfaces in rock: bedding, schistosity, cleavage, and stylolites, which are surfaces of weakness that can be used by the process of fracturing, or for some cleavage and stylolites, may have initiated along pre-existing fractures. This definition of fracture does not require any knowledge of or assumptions about the amount of offset across the opposing faces. The opposing faces of fractures may be in partial or complete contact, may gape open, or may be healed. A FAULT is a fracture whose opposing faces have demonstrable shear offset with or without opening. A JOINT is a fracture whose opposing faces have demonstrable normal-opening offset without shear.

Many fractures exhibit both shear and normal opening, and therefore an investigator must define lower limits on the amount of shear offset that distinguish a fault from a joint. We suggest that if the shear component of the offset is greater than the normal component the term fault be used, and the term joint otherwise. Fracture is the general term and should be used when the details of the offset cannot be demonstrated. Our experience is that usually the relative magnitudes of the components of the offset cannot be demonstrated in the field because of a lack of visible markers cut by a fracture. We will use the terminology presented above throughout the text in order to reduce the confusion that can arise from less-well-defined and mechanistically defined terminologies.

FLUID-FLOW IN FRACTURED ROCKS

Theoretical Approaches

From a hydraulic point of view, a fractured rock mass can be regarded as consisting of two components: (1) intact rock blocks separated by (2) fractures. In general, the network of interconnected fractures serves as the main conduit for fluid flow. The rock blocks, on the other hand, may be permeable or impermeable. If the blocks are permeable, fluid in the blocks will interact with fluid in the fractures. Impermeable blocks do not play a direct role in the fluid-flow process.

Currently, the theory of fluid flow in fractured rocks is still being developed. Various theoretical models differ in the mathematical treatment of fractures and rock blocks. The two extreme approaches can be classified as the discrete and the

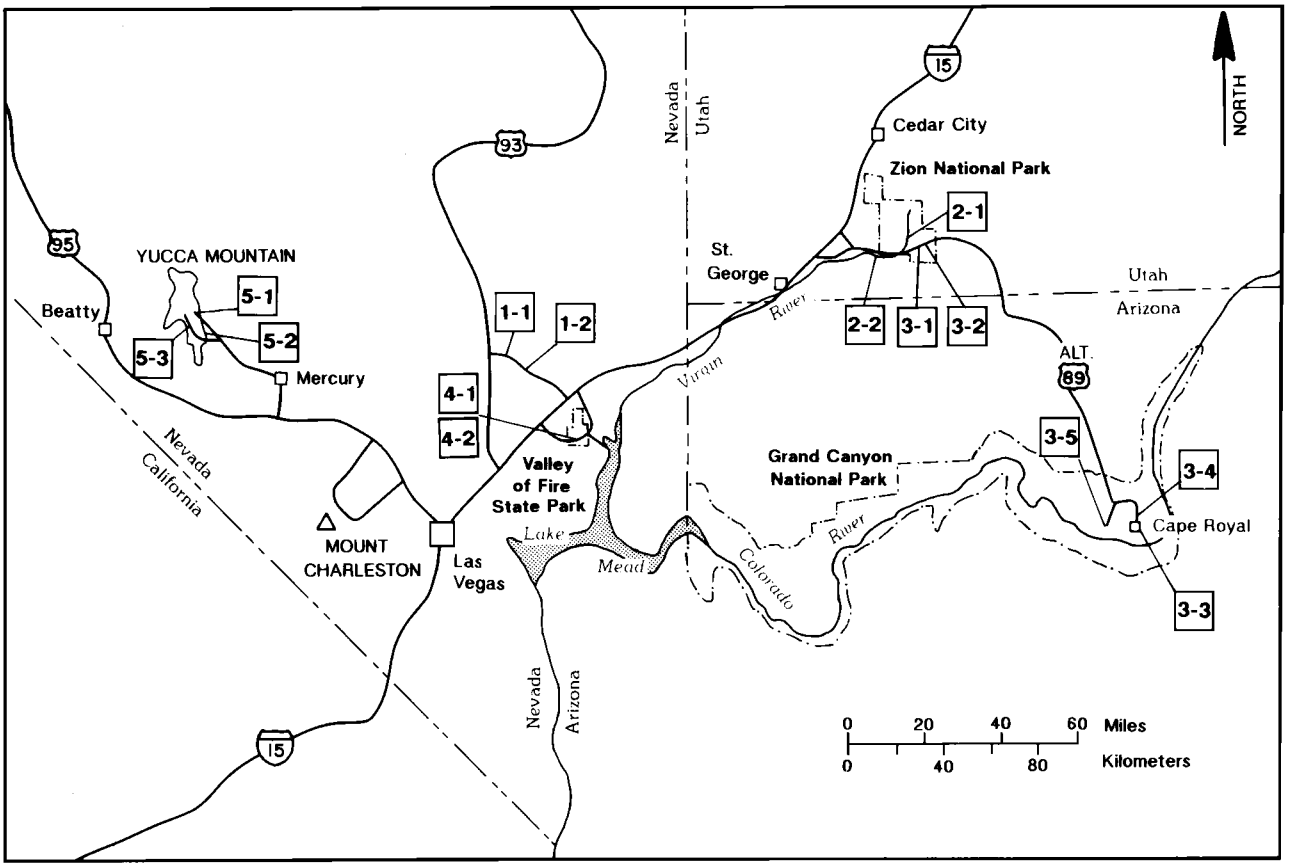

FIGURE 1. Index map showing the locations of field trip stops. Numbers are day-stop.

continuum approaches. Most applications, however, involve elements of both approaches.

Discrete Approach

The discrete approach requires understanding of the fluid flow process in an individual fracture. Theoretical investigation of this process is usually accomplished by representing the fracture as a conduit formed by two parallel plates. Fluid flow is assumed to be steady, viscous, and laminar. Under these assumptions, solution of the Navier-Stokes equation leads to the well-known cubic law, which states that, for a given hydraulic-head gradient, the discharge through a smooth-walled fracture is proportional to the cube of the fracture aperture. Gale and others (1985) reviewed the cubic law and the fluid-flow process in an individual fracture and proposed an empirical factor to account for roughness of the fracture wall. In a more recent review, Cook (in press) proposes exponents greater than three and less than six to fit laboratory tests of flow through rough-walled fractures in rock.

The notion of fracture aperture has created substantial controversy among researchers in the field of fractured-rock hydrology. It is now generally accepted that the hydraulic aperture, i.e., the aperture used in the cubic law, may be different from the mechanical aperture, i.e., the separation distance between the walls of the fracture as measured by a ruler or other mechanical device. Furthermore, these two apertures differ from the transport aperture, which is used to calculate the velocity at which a dissolved chemical is transported through the rock. Recently, this concept of fracture transmissivity has seen use as an alternative to the cubic law and fracture aperture. Fracture transmissivity is defined as the volumetric flow rate per unit length of fracture under a unit hydraulic gradient. Thus, fracture transmissivity is defined from a flow-hydraulic point of view, much the same as hydraulic conductivity is defined for a porous medium. However, there is at present no general agreement on the most appropriate way to characterize the hydraulic properties of an individual fracture.

To apply the discrete approach, the geometry (orientation and spatial extent) and the hydraulic property (transmissivity or aperture) of the fractures must be known deterministically or stochastically. Generally, the deterministic treatment is useful if the number of fractures in the rock mass is sufficiently small that they can be exhaustively sampled. Flow through the fracture network is determined by modeling flow through individual fractures by numerical techniques such as finite

elements. If the number of fractures in the rock is large, data requirements for a deterministic treatment will be overwhelming and a stochastic treatment may be more tractable. In a stochastic treatment, synthetic fracture networks are generated that have the same statistical properties as the fracture network in the field. Again, fluid flow through the synthetic network is determined by computer methods. To examine the variability in flow from one synthetic fracture network to another, numerous networks are generated from the same statistical distributions, and the results are analyzed from a statistical, probabilistic point of view (Monte-Carlo analysis). An example of this approach is given by Andersson and Dverstorp (1987).

Continuum Approach

In the continuum approach, the network of fractures is represented by a fictitious continuum. If the blocks are permeable, they are represented by another continuum, which overlaps and interacts with the fracture continuum. This is known as the double-porosity model and is reviewed by Streltsova-Adams (1987). If the blocks are impermeable, the fractured rock can be represented solely by the fracture continuum. The mathematical treatment of such a single-porosity system is identical to the porous-media flow theory commonly used in ground-water hydrology. The medium may be treated as isotropic, in which case hydraulic conductivity is a scalar quantity, or anisotropic, in which case hydraulic conductivity is a second-order tensor. Where fractures occur in subparallel sets, the hydraulic conductivity of a fractured rock is likely anisotropic.

The continuum approach is justified for porous media because measurements of quantities such as hydraulic head, porosity, and hydraulic conductivity represent averages over many pores. By defining the values of these quantities at a point to mean the average of these quantities over a finite representative volume surrounding that point, it is possible to represent these quantities as continuous functions in space. This concept of representative elementary volume, or REV, is discussed by Bear (1972). In essence, by averaging over the REV, pore-scale variations are smoothed out. Thus, the measured quantity should not be sensitive to small changes in the scale of the measurement.

The concept of REV is problematic when applied to fractured rocks. Field measurements are often limited to boreholes, which intersect small portions of each fracture. When fracture spacing is large, a borehole may intersect only a few fractures. Compared to the porous medium case, this would be equivalent to sampling on a length scale of a few pore diameters. As a consequence, the sampled quantity may be highly sensitive to the scale of measurement. In some cases, the appropriate REV may be so large that field measurements on that scale may be impossible or important details are lost. In these cases, a strict interpretation of the continuum approach would not be useful.

Despite this shortcoming, the continuum approach is widely adopted in studies of fractured rock hydrology. Undoubtedly, one reason for its popularity is the many mathematical tools that have been developed for porous-media flow. Current thinking is to side-step the issue of REV, and to base the scale of investigation on the scale at which practical measurements can be made in the field. Variations in properties such as hydraulic conductivity will be accounted for explicitly as heterogeneity. Thus, the properties of major, important fractures will have to be individually investigated in the field. In the flow analysis, these major features will be embedded in the network of minor fractures represented by a continuum. Such an approach would take on elements of both the discrete and continuum approach.

Recently Neuman (1987) suggested a stochastic continuum approach as an alternative to the REV concept. The rationale behind this approach is that if rock properties are measured over distances smaller than the REV, then they should be analyzed statistically. The analysis is based on geostatistical concepts, and provides a framework to jointly analyze data obtained on different scales. Based on results of hydrologic investigations at a field site in Arizona, Neuman suggested that hydraulic properties over large distances can be inferred from a number of tests over small distances. However, the general applicability of the stochastic-continuum approach awaits further verification.

The patterns of two-dimensional porous-media flow fingering and fracture-trace networks are found to be fractal in both space and time by Maloy and others (1985) and Barton and others (1986). This means that both scale by a power-law to a fractional power, and do not scale linearly as assumed in the REV concept.

Hydraulic Testing

Hydraulic testing, by which water is withdrawn from or injected into a borehole, remains a basic method for determining the hydraulic properties of fractured rock masses. A large body of knowledge has accumulated for analyzing pumping tests in aquifers, and special methodologies have been developed for fractured rocks. These tests are generally known as packer tests because they involve the use of inflatable borehole packers to isolate portions of boreholes for testing and monitoring. Packer tests may be categorized as single-hole and cross-hole. Single-hole tests are performed on packed-off intervals in a single borehole. In a cross-hole test, fluid is injected into (or withdrawn from) a packed-off interval in one borehole, while hydraulic head is monitored in packed-off intervals in neighboring boreholes.

The single-hole packer test has traditionally served as the field method for hydraulic

investigation of a rock mass. Although single-hole tests are simple to conduct, they can investigate the rock mass only in the immediate vicinity of the test interval. Furthermore, single-hole tests are not very suitable for investigating anisotropy. As noted earlier, fractures often render the hydraulic conductivity of the rock mass anisotropic. To overcome these difficulties, cross-hole tests have been developed recently to permit investigation of the hydraulic properties over larger distances and to examine the relationship between fracturing and anisotropy.

The design and operation of packer tests generally depend on the type of information needed for modeling of fluid flow through the rock mass. If the discrete approach is adopted, short test intervals are needed to isolate individual fractures. Packer tests are used to determine fracture transmissivity (from which a hydraulic aperture can be computed), and to investigate fracture orientation and interconnectivity between wells. An example of this application is given by Gale (1975). If a continuum approach is adopted, longer test intervals are needed to sample larger portions of the rock. Single-hole tests are conducted at successive test intervals in a borehole to obtain a hydraulic conductivity profile. Information obtained from these tests may be used in stochastic analysis as proposed by Neuman (1987). Cross-hole tests are used to determine the hydraulic conductivity tensor of the rock. The theory and application of cross-hole tests are given by Hsieh and Neuman (1985) and Hsieh and others (1985).

FRACTURE CHARACTERISTICS

A quantitative understanding of fracture flow requires a quantitative understanding of the fracture characteristics presented below. While orientation, surface roughness, aperture, and mineralization can be measured in rough, natural rock outcroppings, it is desirable to measure all the parameters listed below at the same location. In order to do this, Barton and Larsen (1985) developed the pavement method of clearing a subplanar surface and mapping the fracture network in order to measure the parameters connectivity, trace length, density, and fractal scaling in addition to orientation, surface roughness, aperture, and mineralization. The pavement method will be discussed at Stops 4-2, 5-1 and 5-2. Each of the characteristics is presented below with quantitative examples selected from stops visited on this trip.

Orientation

Orientation has historically been considered the single most important characteristic of fractures. Where a number of fractures share a small range in orientation they are said to form a set. As will be seen on this trip, fractures often do not fall into well-defined sets. Also, all fractures grouped into a set based on orientation are not necessarily of the same generation nor formed in the same event.

The orientation of each fracture is determined by measuring the azimuth and dip using a compass. Normally the azimuth is measured by placing the compass on an exposed portion of the fracture face. However, some volcanic and metamorphic rocks are locally highly magnetized, and deflection of the compass needle can result in incorrect azimuth readings when the compass is placed against a fracture face. At exposures of such rocks, the azimuth should be read after carefully moving the compass several meters away from the fracture surface and the rocks.

Generally, repeat measurements indicate that the azimuth readings are precise to ±2°; dips are precise to ±1°. The poles to fracture and joint planes and to foliation or bedding are plotted on lower-hemisphere equal-area projections. The density of the poles can then be contoured on the projection. In order to provide the reader with the most informative projection we recommend showing both the poles and contours on the projection as shown in figure 2.

Fracture-Surface Roughness

Fracture-surface roughness is an important characteristic in hydrologic modeling because it controls the aperture variation, and thereby, the channeling of flow between the fracture walls. Roughness is important in geomechanics for calculating the shear strength of a fracture (Barton and Choubey, 1977) and the closure stiffness under normal loads (Brown and Scholz, 1985). Roughness is also useful in paleostress analyses for grouping fractures with a common mechanical and temporal origin (Barton, 1984).

Fracture-surface roughness is measured where an unweathered surface can accommodate a 15-cm-long contour gauge. This device (fig. 3) is composed of 148 pins, each about 1 mm in diameter. The pins are held in place by frictional force between two rigid plates. The pins are movable so that when the copier is pressed against a fracture surface the pins adjust to mimic the surface. When the copier is removed from the surface, the pins retain the profile of the fracture roughness. Examples of fracture surface-roughness profiles taken from two sets of fractures at Stop 2-2 at Rockville, Utah, are shown in figure 4. Visual inspection of the profiles reveals that the two fracture sets have distinctly different roughness characters. The roughness is expressed by the roughness coefficient (RC). The RC is most readily determined by visual comparison with a standard set of profiles of known RC, which range (as integer values) from 0 to 20 (Barton and Choubey, 1977; fig. 8b).

At Yucca Mountain, Nevada (Stops 5-1 and 5-2), RC ranges from 1 to 18 and is precise to ±2. The RC for the combined fractures and faults ranges from 3 to 18 and is normally distributed with a peak

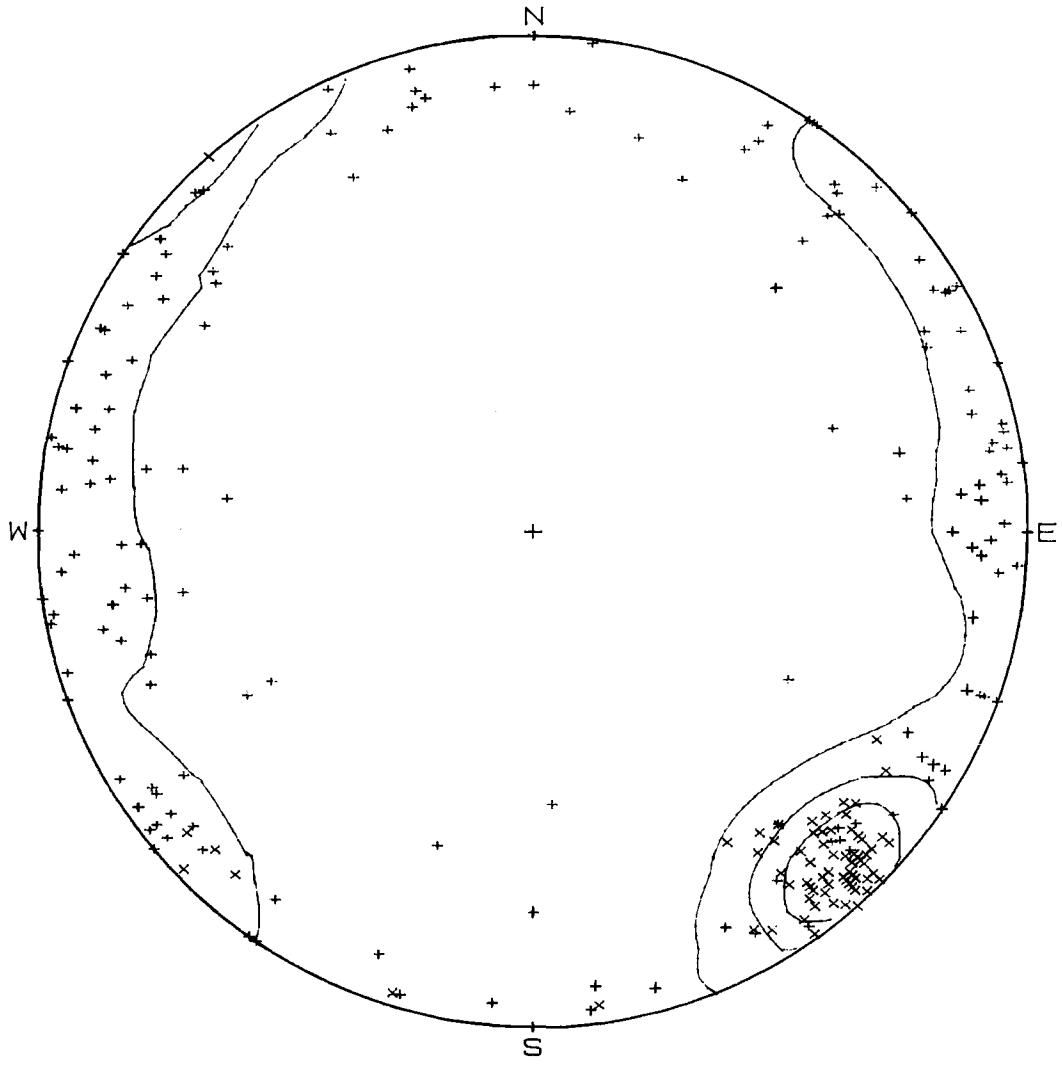

FIGURE 2. Contoured lower-hemisphere equal-area projection of poles to joints and fractures mapped on pavement 100 at Yucca Mountain, Nevada.

at RC = 10. The RC for the joints, however, ranges from 1 to 4 and is also normally distributed with a peak at RC = 2. The narrow range of RC for the joints suggests that the joints share a common mode and time of origin that is distinctly different from that of the fractures. As we will see at Stop 5-1, the joint surfaces contain tubular structures and quench textures and thus are due to cooling (Barton, Howard, and Larsen, 1984). The remaining fractures are due to later tectonism.

Fracture Aperture

Aperture is extremely important in evaluating the flow characteristics of a fracture. For smooth-walled fractures, the volumetric flow rate is a function of the aperture cubed. For rough fractures, Cook (in press) reports that the volumetric flow rate in laboratory specimens of rock to be a function of the aperture to a power greater than three but less than six. The functional dependence of flow rate on aperture for rough fractures is a topic of much study at present, as is the functional relation between hydraulic aperture and mechanical aperture. We report here on the mechanical aperture. We recognize that the removal of overlying rock and exposure to surface weathering has affected the apertures. In contrast, apertures measured underground are affected by stress redistribution and concentration around the walls of the excavation and by blasting. It is not possible to measure mechanical apertures that are unaffected, either at the surface or underground. Our view is that an imperfect measure of aperture is preferable

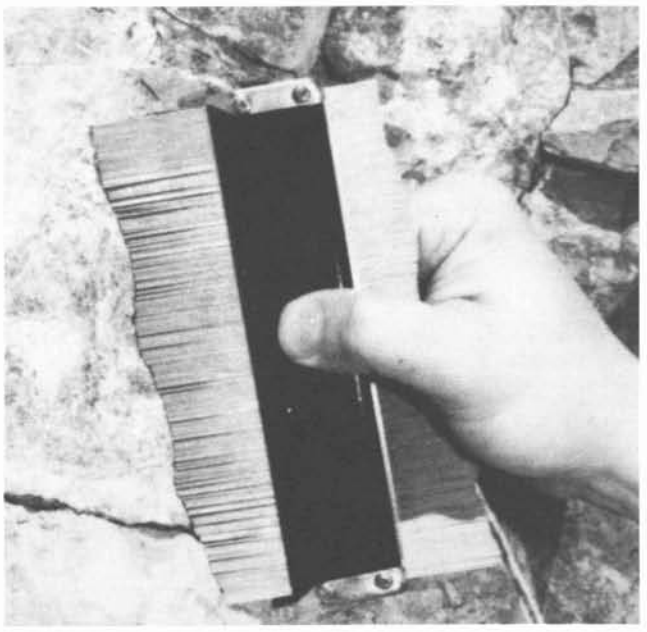

FIGURE 3. Contour gauge used to record fracture-surface roughness.

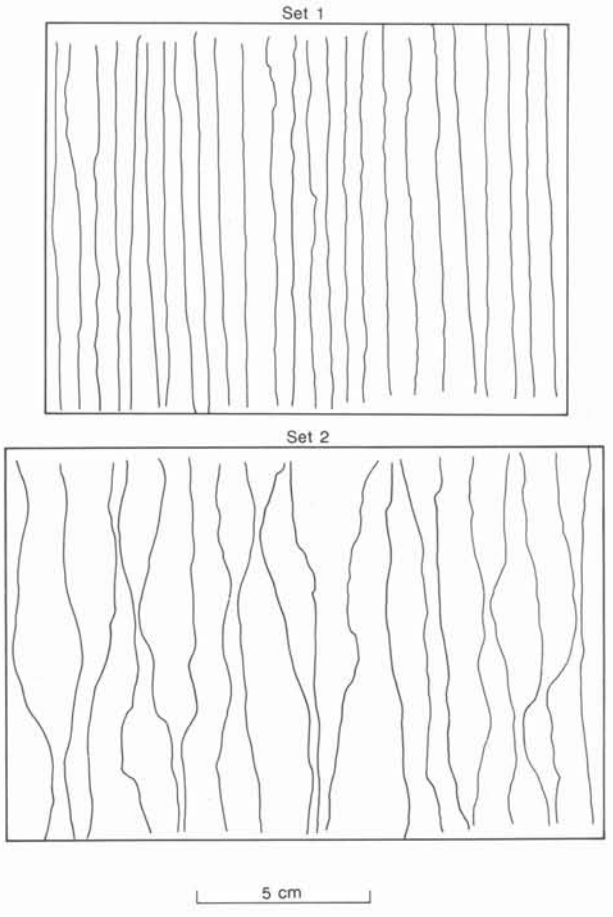

FIGURE 4. Profiles of fracture-surface roughness measured for two fracture sets at Stop 2-2, Rockville, Utah.

to no measure. We suggest that regional unloading due to erosion affects the exact values but not the form of the aperture distribution. This suggestion is supported by scaling analysis of aperture frequency for apertures fixed at depth by mineralization, as discussed below in the section on fractal geometry.

A representative aperture is determined by visual inspection at places where weathering was minimal and mineralization absent. Aperture is measured with an automotive feeler gage or a ruler. Aperture frequencies for pavements 100, 200, and 300 (Stop 5-1) at Yucca Mountain, normalized by dividing the number in each interval by the total number measured at a station, are plotted in figure 5. We have attempted to fit exponential, logarithmic, log-normal, and power-law functions to the tops of histograms of aperture frequency. The histograms are best fit by a power law of the form $y = ax^b$, where y is the frequency, x is the aperture, and a and b are constants. The exponent b is -1.10, -0.87, and -0.99 for pavements 100, 200, and 300 respectively.

Azimuthal anisotropy in aperture is of interest because it contributes to anisotropy in the hydraulic conductivity of the fracture network and in the bulk geomechanical properties. The apertures have opened in response to local and regional tectonic and topographic stresses that caused and subsequently reactivated the fractures. Apertures represent only the normal component of opening displacements.

In order to study aperture anisotropy as a function of orientation, we construct a rose diagram to represent a two-dimensional summation of aperture as a function of azimuth. Figure 6 is a typical example from pavement 300 at Stop 5-1 at Yucca Mountain. The length of each petal in the diagram is the sum of apertures open in the direction of that 10° interval, normalized by dividing by the number of fractures that contributed to that interval. The symmetry of the diagram is an artifact of plotting all aperture directions striking between 0 and 180° on the right side of the diagram and then making the left side of the diagram symmetrical. Intervals with zero aperture are those containing no fractures. The directions of slope of the pavement surfaces and the axes of ridges on which the pavements are located, which can affect aperture anisotropy, are also shown on the figure.

The azimuths of the present-day least-horizontal stress measured at or near Yucca Mountain by hydrofracture (Haimson and others, 1974; Stock and others, 1985) and borehole breakouts (Springer and others, 1984) are also plotted on figure 6. There is as much as 60° of variation in the direction of the least-horizontal stress, but all measurements agree that it trends northwest. This conclusion is further supported by an analysis of earthquake focal mechanisms in the region (Rogers and others, 1983) which resolves the least-horizontal stress to be between 290° and 310°.

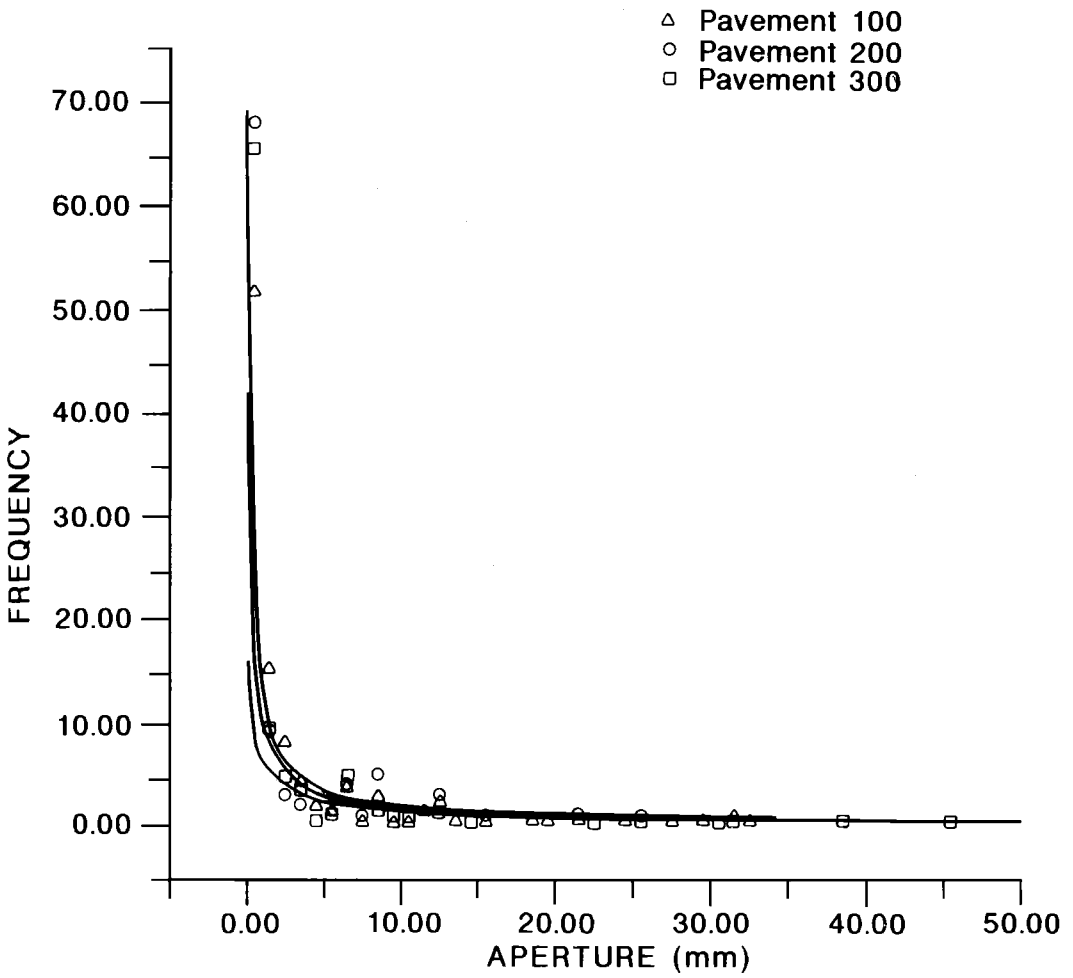

FIGURE 5. Frequency of fracture aperture for pavements 100, 200, and 300 at Stop 5-1, Yucca Mountain, Nevada. Note that axes are offset from origin.

Inspection of figure 6 indicates anisotropy in fracture apertures, but interpretation is difficult. Azimuth of maximum opening is northwest-southeast and falls within the range of the in situ least-horizontal stress, and therefore, we suggest that there may be a direct relation between the two.

Fracture-Trace Length

Fracture-trace lengths are measured from pavement maps (discussed below) or directly on the pavement surface. Frequencies are normalized by dividing the number of lengths in each azimuthal interval by the total number measured on the pavement. Examples from pavements 100, 200, and 300 (Stop 5-1) at Yucca Mountain are plotted on figure 7. The plots include the exposed lengths of fractures whose traces extend beyond the edges of the pavement. Truncation affects the exact values, but not the overall form of the distribution as explained below. The lower end of the distributions are truncated because no trace lengths less than 0.20 m were mapped. The upper end is truncated because many trace lengths exceed the dimensions of the pavements. As with aperture, we attempted to fit exponential, logarithmic, log-normal, and power-law functions to the tops of trace-length frequency histograms. The histograms are best fit by a power law of the form $y = ax^b$, where y is the frequency, x is the trace length, and a and b are constants. The exponent b is -1.17, -0.84, and -1.32 for pavements 100, 200, and 300 respectively.

In order to test the validity of including fractures whose traces extend beyond the pavement boundary, we also fitted curves to only those fractures completely contained within the pavement boundary. Again, the data were best fitted by a power law. Values of b were within 5 percent of the values when all the fracture traces were included.

Segall and Pollard (1983a and b) mapped fracture traces on two pavements in the Mount Givens Granodiorite in the central Sierra Nevada Mountains of California. They also fitted the trace-length frequency distributions with a power law. In

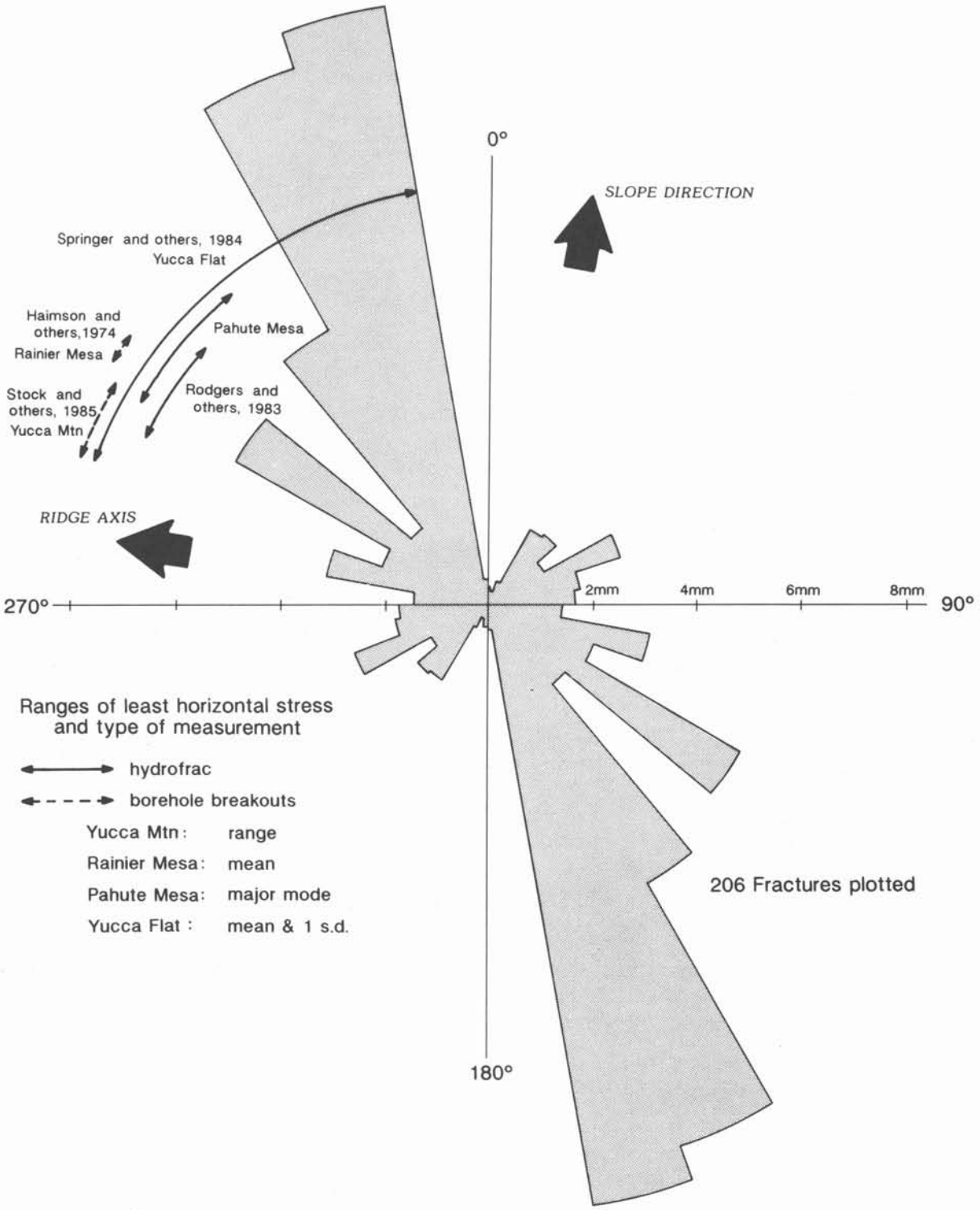

FIGURE 6. Aperture as a function of direction of opening (N.B.: Opening is perpendicular to fracture azimuth) for pavement 300 at Stop 5-1, Yucca Mountain, Nevada.

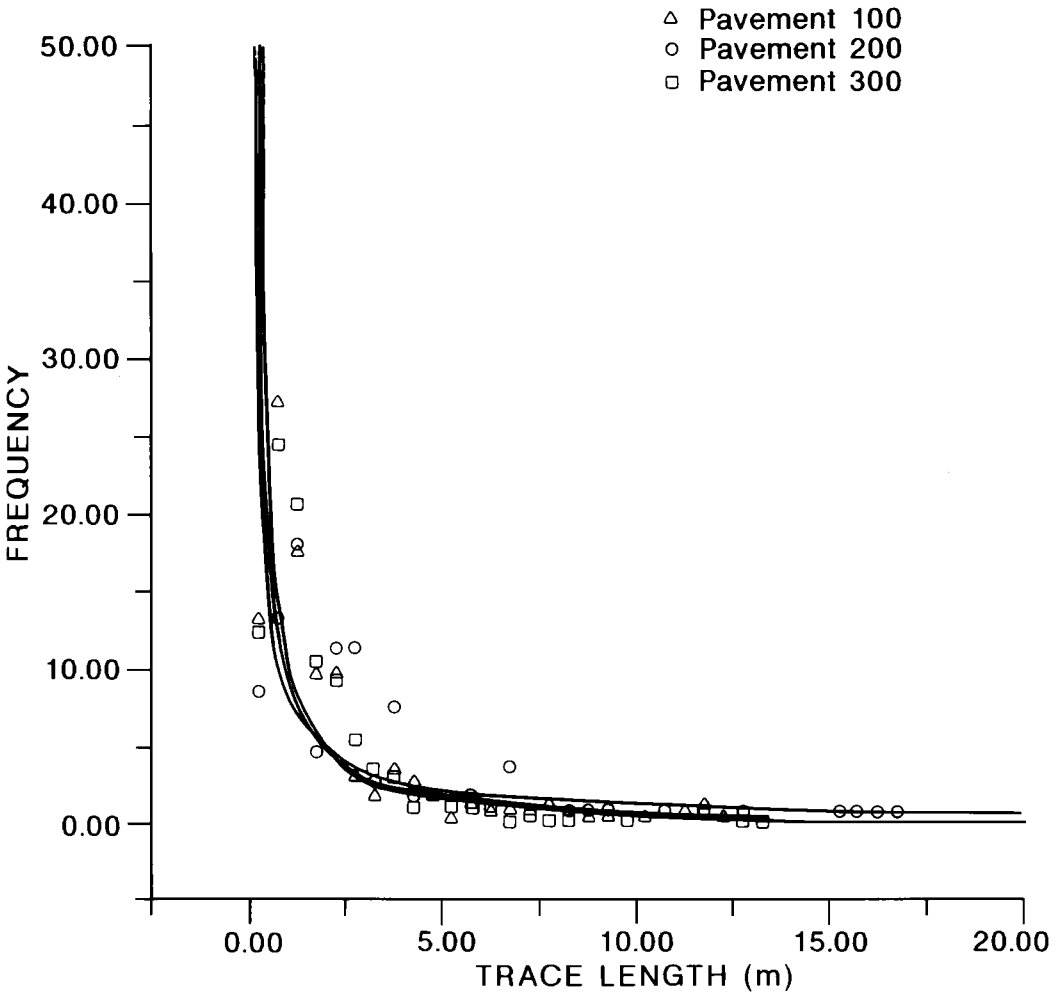

FIGURE 7. Frequency of fracture-trace length for pavements 100, 200, and 300, at Stop 5-1, Yucca Mountain, Nevada. Note that axes are offset from origin.

order to compare our results with theirs, we have fitted their data following the method described above. For their data b equals -0.66 and -1.46. Our values of b at Yucca Mountain range from -0.84 to -1.33. In contrast to our study of networks composed of fractures of many generations and orientations, only one generation of subparallel fractures is present at their sites. The lower end of their distribution is truncated at 2 m, whereas ours continues downwards another order of magnitude to 0.2 m. The same power-law form and similar values for the exponent b for both studies suggests that trace-length frequency is controlled by geometric aspects of the fracture process that are independent of rock type, age, and tectonic history.

Examination of fracture traces longer than 1 cm at the pavement sites at Yucca Mountain qualitatively revealed very large numbers of small fractures that are not visible to an observer from a standing position. Conversely, we have been able to follow the traces of only a few of the long fractures for tens of meters beyond the boundaries of the pavements. These qualitative observations suggest to us that extrapolation along the power-law curves to smaller and longer traces is reasonable. A scaling analysis of trace-length frequency will be discussed below in the section on fractal geometry.

We find no correlation between fracture-trace length and aperture. Such a correlation might be found for isolated non-intersecting fractures, but should not be expected for networks of interconnected fractures.

Fracture Density

The density of fracturing is a parameter used in generating synthetic fracture patterns for hydrologic and geomechanical modeling. An areal fracture density can be expressed in terms of the sum of fracture-trace lengths per unit area of pavement surface. The fracture densities measured at seven pavements at Yucca Mountain range from 0.82 to 5.03 m^{-1}.

Some areas of fracturing on the pavements at

Yucca Mountain are so intense that it is not possible to show each individual fracture on the pavement maps. These areas are identified by stippling (see figs. 15, 16, and 17); short line segments indicate the representative azimuth of the fractures within each area. Some of these areas are bounded by one or more faults (for example, fractures a, b, and c on pavement 100 (fig. 15). We conclude that the intense fracturing of wedge-shaped areas bounded by faults was induced by space problems resulting from displacement along the faults. The other areas of intense fracturing are not clearly attributable to fault displacements.

Fracture Mineralization and Alteration

Minerals deposited on fracture faces can be useful for determining the relative timing of fracturing and for the paleohydrology of a fracture network. As an example, at Yucca Mountain, a few of the fractures exposed on the pavements exhibit mineral coatings, some of which completely fill the aperture. Hand lens inspection showed what appear to be vapor-phase quartz crystals coating two joints on pavements 100 and 300. The coating is light orange brown due to intergrowth of the silica crystals with oxide minerals (Carlos, 1985). Visually similar coating commonly lines the surfaces of the lithophysal cavities and the tubular structures on the surfaces of the joints. If these are vapor-phase quartz crystals, then they were most likely deposited during degassing of the tuff. This suggests that the joints formed very early, soon after emplacement of the tuff.

Calcrete at Yucca Mountain consists of angular tuff fragments and sub-angular calcite fragments cemented by a sugary calcite matrix. A calcrete deposit can be observed bridging fracture d on pavement 100 (fig. 15). The calcrete overlies a white calcite coating, which lines the fracture walls, suggesting that the fracture may have been reactivated and later filled by the calcrete. Calcrete also fills depressions in all three of the pavement surfaces. These calcrete deposits are believed to arise from dissolution and reprecipitation of windblown carbonate in evaporating rainwater pools that collect on the bedrock surface beneath the debris cover, thus incorporating the tuff fragments.

Scattered dendritic deposits of ferro-manganese oxides and hydroxides can be observed on many of the fracture surfaces as well as on much of the pavement surfaces and within the rock matrix. They are small two-dimensional tree-shaped dark-brown to black deposits. These deposits precipitate from solution and are found throughout the volcanic section at Yucca Mountain (Scott and Castellanos, 1984; Spengler and Chornack, 1984, Carlos, 1985; Zielinski and others, 1986), suggesting that surface water has percolated both along fractures and through the rock matrix.

In three areas of fracture intersection on pavement 200 and in one area on pavement 300, the tuff matrix has been altered by water to saprolite. These areas were excavated during clearing of the pavements and were observed to rapidly accept large quantities of water. They may be conduits for rapid movement of large quantities of water from the surface into the interior of Yucca Mountain. We term them black holes.

Fracture Connectivity

The fluid-flow properties of a fracture network are affected by the degree to which the fractures are interconnected. Fractures that are not interconnected can not contribute to fracture flow. Connectivity can be represented by the ratios of the three types of fracture termination or interaction. Fractures may (1) terminate in the rock matrix; we term these blind endings. Alternatively, they may (2) cross or (3) abut other fractures. The percentage of fracture terminations and crossings for pavements 100, 200, 300, and 1000 mapped at Yucca Mountain are shown on figure 8. Blind endings and crossings are found in nearly equal proportions in pavements 100, 200, and 300, but abuttings are found most frequently in all four pavements. The network of fractures in pavement 1000 is highly interconnected and, thereby, highly conductive.

FRACTAL GEOMETRY OF THE FRACTURE NETWORKS

Fracture networks in rock are present from the largest faults down to micro-fractures. The contribution of fracture networks to fracture flow, mechanical stability, and physical properties of rock is not a function of the fractures at any one particular scale, but rather the sum of the contributions of fractures at all scales. Therefore, it is useful to know quantitatively how fracture networks scale over a wide range of scales. Fractal geometry has been applied to quantify complex patterns in nature (Mandelbrot, 1982). Fractal geometry applied to the two-dimensional fracture-trace networks mapped on the pavements simultaneously quantifies the spatial, trace-length, density, and orientation distributions (Barton and Larsen, 1985; Barton and others, 1985 and 1986).

The concept of fractal geometry is particularly useful for investigating scaling of complex objects if they are statistically the same (or self-similar) over a wide range of scales. Fractal objects or processes possess dilation and reduction symmetry. Our previous work has shown that the fracture networks we have mapped are self-similar over the range of scales that can be sampled on a pavement (Barton and Larsen, 1985). We have also found that the pattern of faults mapped by Scott and Bonk (1984) at Yucca Mountain are self-similar (Barton and others, 1986) over the range of scales that can be sampled on their map.

We have greatly improved the technique we have used in our previous papers for determining

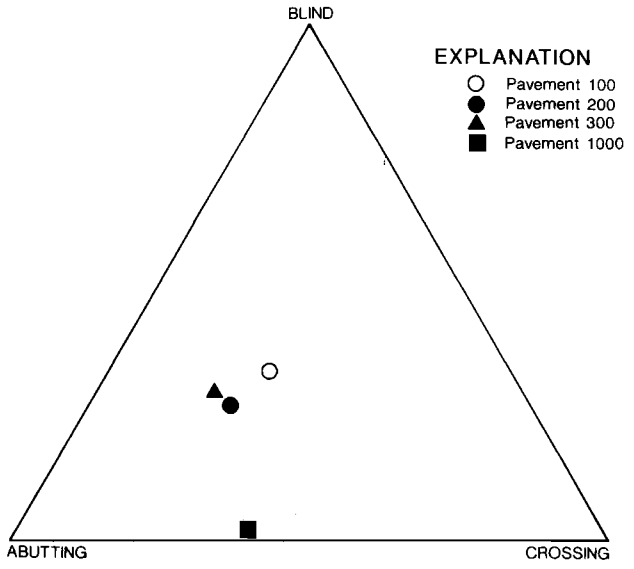

FIGURE 8. Ternary diagram of percentages of fracture intersections and terminations for pavements 100, 200, and 300 at Stop 5-1, and pavement 1000 at Stop 5-2, Yucca Mountain, Nevada.

the fractal properties of fracture networks. Computers permit us to easily sample a greater number of intermediate scales than we could for our earlier papers and thereby to more finely sample the fractal behavior and determine the fractal dimensions of the networks.

We use an adaptation of the box method of fractal analysis where grids of various-sized square cells are placed successively over the maps, and the number of cells intersected by fracture traces counted. The fractal distribution of lines on a map is:

$$Nr^D = 1$$

or equivalently

$$D = \log N/\log(1/r)$$

where N is the number of cells containing portions of one or more fracture traces, r is the length of the side of the cell, and D, the fractal dimension, is the slope of straight-line segments fitted to the N,1/r points plotted on logarithmic axes.

Our recent unpublished investigations of the box method for determining the fractal properties of an object reveal that the method is particularly sensitive to the orientation of the grids. We now know how to overlay the grids to obtain the minimum N for each cell size and thereby obtain the fractal dimension with an accuracy of + 0.05. Our investigations of the box method also indicate that the range of cell sizes for sampling the fractal properties of a fracture network is limited by the network itself. The smallest cell size should be no smaller than the shortest fracture in the network, while the largest cell size should be smaller than the size at which all the cells are occupied. With this clearer understanding of the limits and accuracies of the box method, we have measured the fractal properties of the networks mapped on pavements 100, 200, and 300, and 1000 as shown in figure 9, where the log of 1/r is plotted versus the log of N for each cell size. The fractal dimensions of all three networks lie between 1 (the dimension of a straight line) and 2 (the dimension of a filled plane), with confidence levels of 0.99.

Because the points can be fitted by smooth lines (either straight or curved), the networks can be said to be fractal over the range of r sampled. Because these lines are straight (not curved), the networks can also be said to be scale independent over the same range. The fractal dimension is a quantitative measure of scaling. Barton and others (1986) have shown that the network of faults mapped at 1:12,000 by Scott and Bonk (1984) has a fractal dimension (plotted on fig. 9) that is very nearly equal to the average of the range of the dimensions determined for eight pavements mapped at 1:50. This suggests that the fractal properties of fracture networks are scale independent over a broad range of scales at Yucca Mountain.

Once the fractal dimension of a pattern or object in nature is determined, it is possible to model that pattern or object starting from a single generator. A generator is the fundamental building block from which a fractal pattern or object is generated by iterative replacement of each piece of the generator by a reduced version of the generator. The task of deducing a generator for a particular fractal pattern observed in nature is not easy. One approach is to guess the generator, as was done by King (1983), for the map pattern of the traces of subsidiary faults in the immediate vicinity of large-scale fault bends. The box counting method has an intrinsic upper limit of 2.0 for the fractal dimension of patterns of lines lying in a plane. Non-overlapping fractal generators that lie in a plane also have an upper limit of 2, while overlapping fractal generators lying in a plane can exceed 2.0. For the ten pavements we have studied, we have not found fractal dimensions of fracture traces to exceed 1.8, and we conclude that their generators are not space filling. In order to simulate fault patterns, King (1983) proposed a three-dimensional space-filling generator but assumed that it was never fully formed. In a two-dimensional section, the equivalent is a fractal dust with a dimension of 1.0 which falls below the values we have measured for the pavements. We commonly observe crosscutting fractures on our maps which suggests that a proper generator for modeling fracture trace patterns should be overlapping. The generator proposed by King (1983) was for shear faults that did not overlap and therefore is not appropriate for the patterns of crossing fractures. We have been unsuccessful at

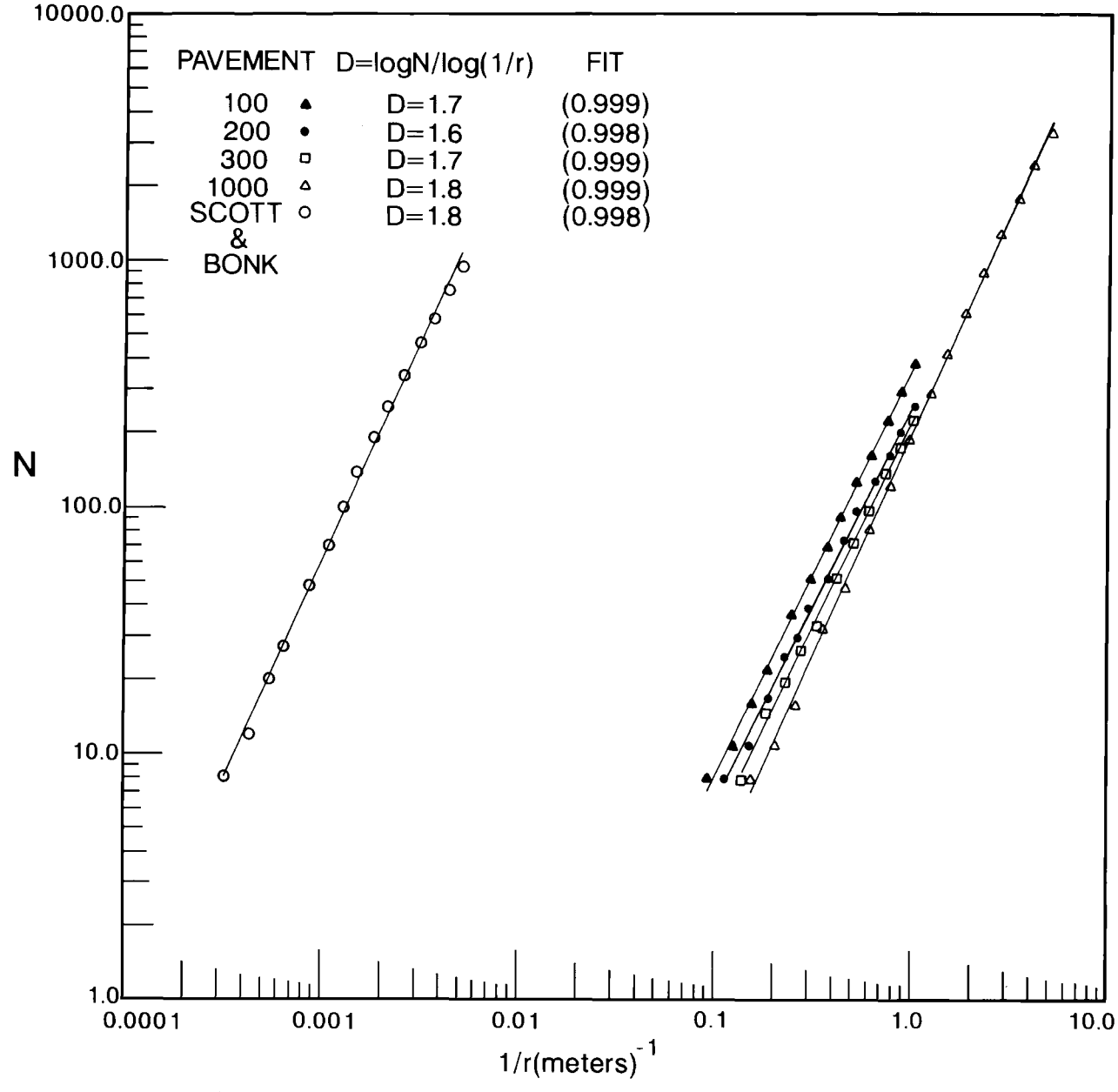

FIGURE 9. Fractal plot for fracture networks mapped on pavements 100, 200, 300, and 1000, and for the fault network mapped by Scott and Bonk (1985) at Yucca Mountain, Nevada.

guessing a generator for modeling our fracture-trace maps. A most promising method for deducing a fractal generator is the iterated function systems approach being developed by Barnsley and Demko, 1985 which systematically deduces a fractal generator for a given fractal object.

The parameters of aperture and trace-length frequency are best fit by power-law distributions as presented above. Thus these parameters are also fit by an equation of the form $Nr^E=1$ where N equals the frequency and r is aperture and trace length respectively. A power-law function of this form is a strong indication of self-similarity and the scaling exponents E are often, but not always, referred to as a fractal dimension. Log-log plots for aperture frequency are shown in figure 10 and those for trace-length frequency in figure 11.

The aperture frequency distribution for each network is best fit by a single line whose slope is a scaling exponent E. The exponent ranges from 0.9 to 1.5 for the gaping fractures exposed in four pavements at the surface of Yucca Mountain. In a pavement from Colorado all the fractures were sealed in situ by quartz mineralization, which preserved apertures as they were at depth. The exponent of these in situ apertures is 1.8, the highest we have measured. Given a network of fractures of various length, the effect of uplift and unloading is

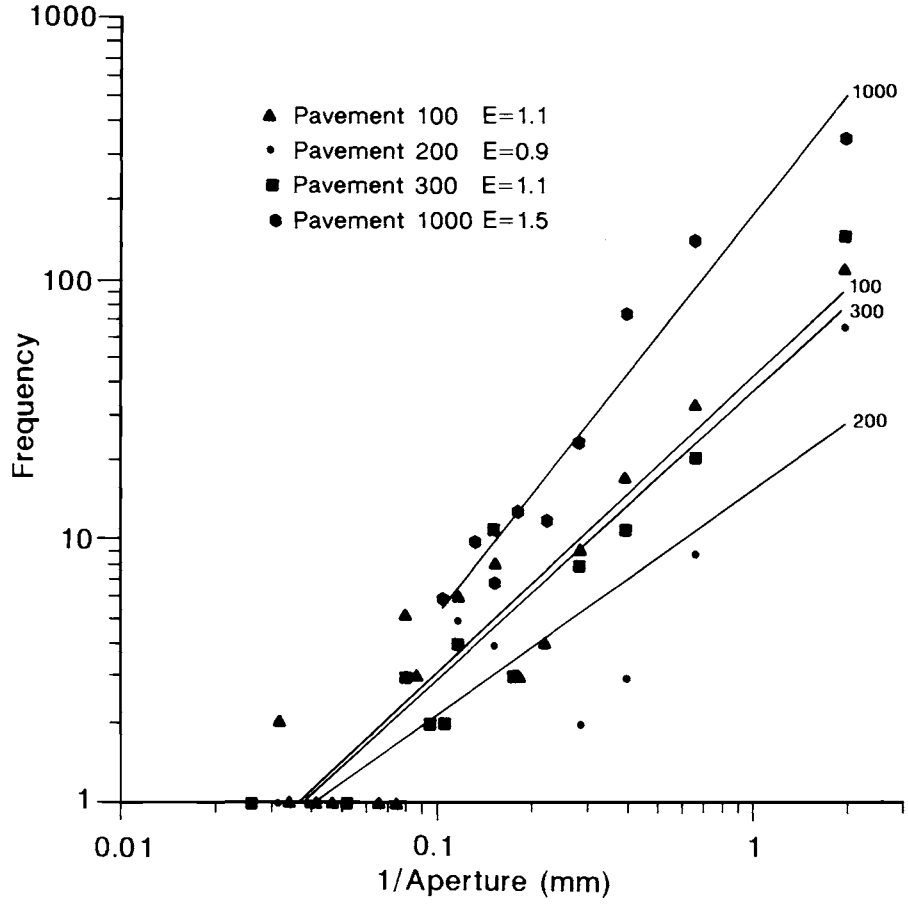

FIGURE 10. Log-log plot of frequency of inverse aperture for pavements 100, 200, 300, and 1000.

to preferentially increase the initially larger apertures because of the greater elastic energy necessary to hold larger apertures closed at depth. The effect of initially large apertures opening more rapidly than smaller apertures during unloading will be to decrease the exponent E. Our data support the view that uplift and unloading lower exponent but do not change the form of the distribution. Based on our data to date, we suggest that the aperture frequency distribution at depth has an exponent greater than 1.5 and that the lower values measured at the surface are probably due to uplift and unloading. We offer no intrinsic upper limit for the exponent for aperture distribution.

Fracture-trace-length frequency distributions for all the pavements we have studied to date have exponents that range from 1.2 to 2.1. A higher exponent means a higher frequency of short trace lengths. The exponent for trace lengths in the Tiva Canyon member at Yucca Mountain ranges from 1.2 to 1.6, suggesting that trace length distributions can vary over small lateral distances. We offer no intrinsic upper limit for the exponent for trace-length distributions.

PATTERN OF DEVELOPMENT OF FRACTURE NETWORKS

Fracture networks become more complex with time as new fracture generations are added to those that already exist. New generations of fractures form during discrete episodes, each of which records a discrete element of the tectonic history. Most episodes of fracturing are not accompanied by major tectonic deformation features such as folds and faults. Where it can be determined that the fractures in a network formed in tension, then it is possible to determine the relative ages of the fractures on the basis of abutting relations (younger fractures abut older ones). This method has been applied to pavement maps at three different geographic localities in three different rock types and tectonic terranes by Barton and others, 1986. One of those localities is Stop 5-1, at Yucca Mtn.

Analysis of some of the fracture properties from one generation to the next reveals the following pattern of fracture network development. In general, the first generation fractures are long and subparallel. Fractures in the next generation are

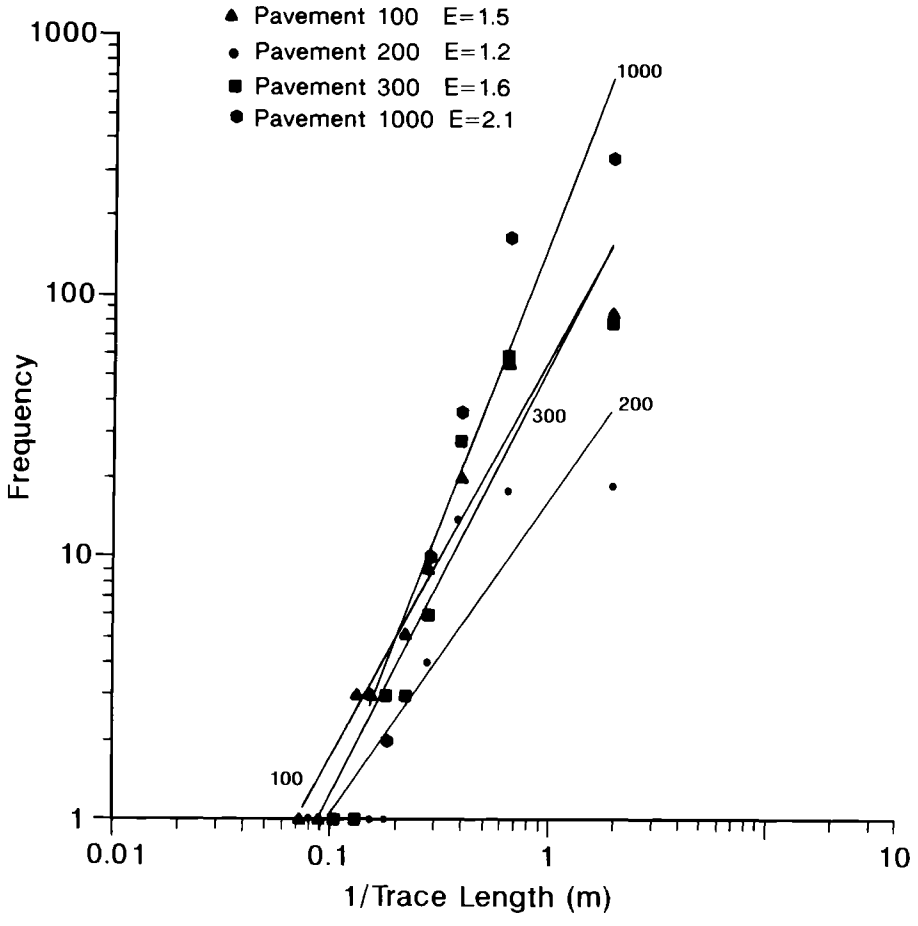

FIGURE 11. Log-log plot of frequency of inverse trace length for pavements 100, 200, 300, and 1000.

shorter, and abut the first fractures generally at high angles, forming large, polygonal blocks. Fractures of the younger groups are generally shorter and more diversely oriented. They form small, irregular polygonal blocks within the larger blocks bounded by the older fractures. The younger fractures appear to have formed in response to local stress conditions within the blocks in which they formed, and thus are less useful for determining regional paleostress orientations.

FRACTURE-FLOW MODELING

The pattern of development for fracture networks described above has been incorporated into a computer program for generating realistic synthetic-fracture networks by Barton and others, 1986. For each generation, the program selects randomly from the distributions of orientation, connectedness, trace-length, aperture, and spatial position measured in the field. The spatial position distribution is fractal, and trace-length, and aperture distributions are power-laws. The fractal approach is further used to scale the synthetic networks from the largest fault down to the microfractures. The networks thus generated are statistically equivalent to those mapped in the field.

The synthetic network (or one mapped in the field) is then input into a two-dimensional fracture-flow computer program which calculates the direction of flow and hydraulic conductivity for each fracture segment in the network. The combination of these two computer codes will permit study of the dynamics of discrete-fracture-flow systems. In the future, site-specific discrete-fracture-flow studies will be based on field characterization of fracture and hydrologic properties sampled at a few points in the system, which will be scaled and interpolated using fractals or some other statistical approach, and input into fracture-flow computer models.

PART II - DESCRIPTION OF STOPS

DAY 1 STOP 1
WILDCAT WASH
(USGS Topographic Map, Wildcat Wash S.E., Nevada, 1969)

Wildcat Wash is cut into the Muddy Creek Formation by the Muddy River/Colorado River

drainage. The Muddy Creek Formation (Miocene) is composed of clay, sand, and conglomerate deposited in a large playa lake or swamp 12-6 million years ago (Ma) (Metcalf, 1982). It is mostly unaffected here by Tertiary extension, except for a few steeply dipping normal faults with small displacements.

As you walk up the dirt road along the floor of the wash, you first pass through lake-bottom carbonate rocks that contain algal deposits and plant root and stem casts. The rocks are interpreted to be lacustrine spring deposits. These tabular deposits (mounds) are thickest near the spring source and thin away from the source. Note the prehistoric pictographs on cliff walls.

Continue walking up the wash and down section. Note transition to conglomeratic facies. In this facies we see the stockwork of carbonate fracture-fill veins that are interpreted to be the feeders to the lake-bottom carbonate deposits we just passed through. The carbonate veins fill a fracture network that is composed of faults and joints. The faults, some with traces as long as 250 m, probably formed by slumping before lithification (note that the conglomerate pebbles in the fault zones are not shattered). Individual fault zones range in width from 0.5 cm to 0.75 m. The orientations of the faults are highly variable, but for the largest faults are approximately N-S, 80°W. A complex network of carbonate-filled joints interconnect the faults and extends downward in size to joints a few centimeters in trace length.

Continue walking up the wash to the contact (at mouth of small canyon) where the Muddy Creek Formation laps onto bedrock limestones and dolomites of the Pogonip Group (Ordovician). Here the Pogonip has been shattered to a breccia. Such shattering is commonly associated with Basin and Range extension. Do not proceed up the small canyon; instead walk 100 m east up the scree slope to examine a 0.75 m-wide carbonate vein in bedrock. Then proceed north 0.3 km across rough terrain, examining carbonate-filled fault and joint networks along the way and ultimately circling around and rejoining the small canyon.

Carbonate which infills the faults ranges from micro-crystalline fill between conglomerate casts to 5-cm-long vug-filling calcite crystals. Vug walls exhibit up to 30 paired laminations of microcrystalline calcite. In some faults, the vugs exhibit a stockwork composed of a "log jam" of laminated fragments up to 8 cm long with fragments of wall rock that broke from the walls and fell into open vugs. The laminations, stockwork of laminated fragments, and wall-rock fragments all indicate repeated reactivation of the faults that prevented the flow system from being sealed.

The network of interconnecting joints between the faults breaks the rock into progressively smaller blocks down to centimeter size. Locally, on the scale of a few meters, the joints often form two perpendicular sets within blocks bounded by larger joints and faults. In places, carbonate fills the entire length of one or both sets of joints. In other places the carbonate fillings follow a zigzag path along parts of two intersecting joint sets, indicating that the flow direction was oblique to both sets (fig. 12). Locally, the flow pattern is very complex and not uniform over volumes larger than an individual fracture.

Rejoin the small canyon and walk north. Observe open flow tubes as much as 40 cm in diameter partially closed by carbonate laminations on east wall of canyon. Continue walking north 500 m and examine oxidation by fluids along a low-angle normal fault (N30°W, 20°NE).

Turn around and proceed south through small canyon, observing stockwork of carbonate-filled veins. At mouth of small canyon, continue walking 1.6 km back to bus.

DAY 1 STOP 2
MUDDY RIVER SPRINGS

(USGS Topographic Map, Moapa West, Nevada, 1983)

Muddy River Springs is a discharge point of a large regional ground-water flow system known as the White River flow system. As defined by Eakin (1966), the White River flow system consists of 13 intermontane valleys within or adjacent to the White River drainage basin in east-central Nevada. The flow system is narrow, trends north-south, and is about 380 km long and as much as 110 km wide with ground water at depths greater than 1 km. For such deep circulation it is reasonable to expect that the topographic boundaries of the individual valleys do not exert a significant influence on ground-water movement. Rather, the flow of ground water integrates the individual valleys into a single, large flow system. This concept of interbasin ground-water flow emerged only during the early 1960's.

Prior notions of ground-water flow in Nevada were based on the assumption that movement of water was more or less restricted within topographically closed basins. Under this concept, water enters the flow system as recharge along the higher elevations at the edge of the basin, flows toward the center of the basin, and discharges by evaporation and plant transpiration (together known as evapotranspiration). While this concept is valid for many basins in Nevada, results of several hydrologic investigations have convincingly demonstrated the existence of large, interbasin ground-water flow systems (Eakin, 1966; Maxey and Mifflin, 1966; and Winograd and Thordarson, 1975).

The main evidence for interbasin flow systems is summarized as follows: 1) Some basins have deep water levels that preclude discharge by evapotranspiration. Recharge into the basin must flow in the subsurface to adjacent basins, eventually discharging some distance away from the originating basin. 2) Hydraulically isolated basins generally have large differences in water-level elevation.

FIGURE 12. Carbonate (white) filling a zigzag path formed by the intersection of two joint sets at Stop 1-1.

However, a number of adjacent basins have similar water-level elevations, which suggests that the basins discharge to a common discharge area. 3) The spring flow in some valleys is substantially higher than could be sustained by local recharge over the basin; thus, part of the spring water must come from other basins. 4) The chemical quality of water in a number of adjacent basins is similar.

Interbasin flow occurs generally over eastern Nevada and westernmost Utah, within a region known as the carbonate rock province. According to Harrill and others (1983), the carbonate rock province is bounded by the Wasatch Range on the east and the Roberts overthrust belt on the west, and extends northward from Lake Mead and the Virgin River to the divide between the Great Basin and the Snake River drainage basin. The rocks in this province contain thick units of limestone and dolomite of Paleozoic age. The intercrystalline porosity of these rocks is extremely low, and ground water flows mainly through secondary openings, such as solution-widened fractures and bedding planes. The rocks have undergone considerable deformation, including Mesozoic thrust faulting and Cenozoic extensional faulting. In places, faults may act as barriers to flow, while in other places, faults may act as highly transmissive conduits. Thus, the movement of ground water is complex and is strongly controlled by structures.

The Muddy River Springs consist of some 15 or more springs in upper Moapa Valley, at the southern end of the White River flow system. The spring water emerges at about 32°C. and discharges into the Muddy River, which drains into the Colorado River. The total spring discharge, as measured by the gaging station on the Muddy River several kilometers downstream from the spring outlets, is about 44 million m^3/yr. Eakin and Moore (1964) analyzed 25 years of discharge records at this station and found a high degree of uniformity in spring discharge. If the springs were fed by local recharge, spring flow should show seasonal variation. The observed uniformity in spring discharge is additional evidence that the spring water is a from a large regional ground-water flow system.

At Taylor Ranch, observe the pool formed by spring discharge. Temperature of the spring water is a constant 32.6°C throughout the year.

DAY 2 STOP 1
WEEPING ROCK SPRING
(Geologic map, Hamilton, 1978)

At Weeping Rock Spring, water emerges from the Triassic(?) and Jurassic Navajo Sandstone. With a maximum thickness as much as 610 m, the Navajo Sandstone is the most important consolidated-rock aquifer in the upper Virgin River basin, which encompasses Zion National Park (Cordova, 1981). Water in the Navajo Sandstone moves primarily through open fracture systems. In Zion National Park, fractures in the Navajo Sandstone are well developed (see cover photograph). Presence of open fractures at depth is indicated by loss of circulation during well drilling near the park (Gates, 1965). Locally, a significant amount of water may also move through intergranular openings.

Where the Navajo crops out, natural recharge takes place by direct infiltration of precipitation, melting snow, and stream seepage. In areas of higher elevations (towards the headwaters of the Virgin River), the Navajo is overlain by Cretaceous and Tertiary rocks. Nevertheless, recharge into these younger rocks may eventually move downward into the Navajo. Underlying the Navajo Sandstone, the less permeable Kayenta Formation is an impediment to further downward movement of water. As a result, water moves laterally through the Navajo, discharging as springs and seeps and into streams.

Weeping Rock Spring is near the base of the Navajo Sandstone, and marks an intersection between the regional water table and the wall of Zion Canyon. Water emerges from the sandstone along fractures and drips down the canyon wall.

Hamilton (1984) noted that Weeping Rock Spring, like other springs in Zion Canyon, is located beneath hanging canyons, which collect recharge to support the springflow below. Hamilton also noted that the spring waters in Zion Canyon are rather alkaline, with concentrations of bicarbonate ranging from 148 mg/L to 98 mg/L. At Weeping Rock Spring, deposits of calcareous tufa can be seen forming on the sandstone wall.

Weeping Rock is so named because of the discharge of ground water from both subhorizontal and vertical unloading fractures in the Navajo Sandstone. The face of weeping rock is created by two large fractures. The large planar face N25°W, 80°SW is an unloading fracture parallel to the canyon wall. The second fracture is the large convex-up, arch-shaped fracture that abuts against the planar face. In early spring, the surface of Weeping Rock is a curtain of water cascading down the surface of the large planar fracture which is covered with green moss and algae. The corrugated texture of portions of the fracture face is formed by tufa deposits from the discharging water. Erosion of the basal 6 m of the exposure by the discharging water has produced the cylindrical undercutting locally called a subway.

Return along footpath to the footbridge. Turn south (left) and hike up steep switchback trail to Echo and Hidden Canyons. This 4.8-km round trip hike takes us 396 m above Weeping Rock to view the vertical fractures in the recharge area. Rain water and snow melt take two years to move down through the fracture network to Weeping Rock. The trail is paved most of the way until you reach the mouth of Hidden Canyon. The trail follows the stream bed into Echo Canyon. Note that Hidden Canyon has formed by erosion enhanced by the presence of a swarm of fractures oriented N12°W along the floor of the canyon. Such fracture swarms are common in the Navajo Sandstone and appear to be responsible for the location and orientation of most of the NNW-trending canyons in the region. Continue along Echo Canyon trail 1.3 km to the intersection with trail to Observation Point, to the north (left). Note swarms of fractures oriented N54°W, 90°, with vertical traces 20 to 50 m long. Because of their long vertical extent and iron staining, these are most likely the fractures along which water locally flows vertically downward to Weeping Rock below. Approximately 3 m beyond the footbridge, excellent examples of blast-induced fractures are present in the cliff wall along the trail; they are identified by their radial pattern concentric about the blast point and their fresh unstained surfaces. Just before the intersection with the Observation Point trail, note iron stains from water seeping out from subhorizontal bedding-plane fractures along the cliff walls across the valley. Retrace route along trail to parking area.

DAY 2 STOP 2
ROCKVILLE, UTAH
(Geologic map, Hamilton, 1978)

To a viewer standing in the cemetery, the view to the north up this unnamed wash is of Mount Kinesava, which is composed of Navajo Sandstone (Triassic? and Jurassic) overlying the Kayenta Formation (Upper Triassic?). The wash is bounded on the east and west by the Rockville Bench, which is capped by the Shinarump Member (grey and white cliff), the basal member of the Chinle Formation (Triassic). We will study the fractures in the massive siltstone units in the uppermost Moenkopi Formation (Triassic) that form the red cliffs beneath the Shinarump Member.

Walk through the cemetery, then northeast up the debris slope to the exposure of large fractures in the 6-m-thick massive siltstone bed in the upper part of the Moenkopi Formation in the cliff face. Two dominant fracture sets are exposed. We will measure and discuss the following characteristics of the fractures in these two sets:
(1) Orientation. Measure strike and dip of 15 fractures in each set and of bedding with your compass. Plot poles to fracture planes on a lower-hemisphere equal-area stereographic projection.
(2) Relative ages. Determine the relative ages of the two sets, using abutting relations.
(3) Spacing. Measure the perpendicular distance sequentially from one fracture to the next in the same set. Do this for each set. Plot results.
(4) Vertical trace length. Do these fractures extend all the way to the top and bottom of the bed? Are they contained within the bed, or do some of them extend into overlying and underlying beds?
(5) Roughness. Take roughness profiles of the fracture faces for both sets. Determine the roughness coefficient by visual comparison with curves of known roughness. Is there any difference in roughness between the two fracture sets?
(6) Draw a schematic 3-D sketch map (block diagram) of the fracture network in this 6-m-thick bed, based on the observations you made above.
(7) Fracture-surface structures (see fig. 13). Note the fracture-surface structures prominently displayed by one of the fracture sets. Note the following features: (a) twist and inclusion hackle, (b) arrest lines. From your observations, comment on the direction of propagation, shape of the fracture front, mode of fracture, and orientation of the stress field relative to the fracture plane.
(8) Examine the fractures for shear offset and determine whether these fractures are joints or faults.
(9) Mineral fillings. Note the presence or absence of mineral fillings and desert varnish. What would the absence of mineral fillings suggest about the position of these fractures relative to the water table

at the time they formed and subsequently? What does this suggest about the time of their formation relative to the uplift of the Colorado Plateau and Tertiary extensional tectonics?

Break up into groups of two and study the eight characteristics listed above as they apply to one of the four siltstone units exposed in the Moenkopi Formation in the cliff across the wash. Note each unit is of different thickness. When you have finished, we will collate the results to see which of the characteristics, if any, are affected by unit thickness.

DAY 3 STOP 1
CLEAR CREEK
(Geologic map, Hamilton, 1978)

Cross road and park in pull-off on north (left) side of Rte. 9. Walk along path approximately 0.3 km to the northwest and climb up to top of small ridge of Navajo Sandstone. Looking to the south across Rte. 9 you will see a 30-m-wide fracture swarm containing approximately 40 subvertical fractures striking N12°-26°W. Note that the swarm extends northward through the ridge you are standing on. Return to parking area, then cross Rte. 9 (caution - traffic) and climb down the embankment of Clear Creek. Walk west along the creek bed to the first side canyon on the south. Look south to the head of this canyon and observe the intensely fractured central 6 m portion of the same fracture swarm you observed from across the road. The fracture swarm controls the erosion that formed this canyon. Measure the orientation of 20 fractures in the swarm. How does their strike compare with nearby canyons and washes? Measure the spacing between the fractures along lines perpendicular to their planes. Does the anastomosing of individual fractures within the swarm affect the spacing distribution or mean? Examine the fractures for evidence of shear offset and determine whether these fractures are joints or faults. Look for mineral deposition or erosion on the fracture faces. Is there evidence of whether these fractures have been the conduits for fluid flow? Return to vehicle.

DAY 3 STOP 2
CHECKERBOARD MESA
(Geologic map, Hamilton, 1978)

Look southwest across road to Checkerboard Mesa, named for the checkerboard-like squares formed by the erosional enhancement of subvertical fractures and subhorizontal cross-beds in the Navajo Sandstone. Cross Rte. 9 and walk west along the road and down the embankment, ford Clear Creek, and continue to the base of Checkerboard Mesa to examine the checkerboard fractures. What is the relation between the cross-beds and the vertically short fractures, and between the cross-beds and the vertically long fractures? Note that the subvertical fractures are primarily perpendicular to the weathering face of the mesa. Thus, the strike of the fractures swings around from northeast to northwest as you walk east around the nose of the mesa. This suggests that the subvertical fractures are not tectonic but instead are caused by exposure. Continue walking east approximately 0.2 km, look back at Checkerboard Mesa, and note that the subvertical fractures are rarely seen on the western exposure. They appear only on the northern end of the mesa and penetrate less than 3 m along strike into the rock. E.R. Verbeek and M.A. Grout (written commun., 1986) described similar fractures of limited penetration exhibiting the same right-angle relation to the contours of small outcrops in the oil shales in Piceance Creek, Colorado and also concluded that such fractures are produced by exposure. Retrace our walking route back to the vehicle.

DAY 3 STOP 3
CAPE ROYAL AT THE GRAND CANYON OF THE COLORADO RIVER
(Geologic map, Anonymous, 1976)

Walk 0.6 km along path to Cape Royal amphitheater overlooking the Grand Canyon for a lecture on the geologic history, structure, and stratigraphy of the canyon given by personnel of the National Parks Service.

DAY 3 STOP 4
ROADCUT OF SANDSTONE UNIT IN KAIBAB FORMATION
(Geologic map, Anonymous, 1976)

This outcrop is cut by many steeply dipping faults with slickensided surfaces. We will measure the attitudes of the fault planes, pitch of the slickenlines, and sense of displacement on these faults. We will then demonstrate how these data can be used to determine the orientation and relative magnitudes of the three principal stresses that produced the fault slip, using the method of fault-slip analysis developed by Angelier (1984).

DAY 3 STOP 5
NORTH RIM LODGE OF THE GRAND CANYON OF THE COLORADO RIVER
(Geologic map, Anonymous, 1976)

Walk 0.5 km down path from the North Rim Lodge to Bright Angel Point for an overview of the Grand Canyon of the Colorado River. Use binoculars to study fractures in the distant walls of the canyon. Note that the fractures are stratabound within individual rock units or packets of units.

DAY 4 STOP 1
MOUSE'S TANK PARKING AREA
(Geologic map, Bohannon, 1983)

The surfaces of fractures in rock are often decorated by a tracery of faint ridges and steps that form radial, concentric, and plume-like patterns (fig. 13) that are collectively termed fracture-surface structures. They should not be confused with slickenside striations and steps which may also be present on fracture. The patterns, morphology, and tensile origin of these structures has been extensively described in Kulander and others (1979); Barton (1983); and Kulander and Dean (1985). We will examine and discuss the mode of origin of magnificent examples of fracture surface structures including hackle lines and steps, twist hackle steps, inclusion hackle, arrest lines, and plumose patterns on fractures in the Aztec Sandstone (Triassic? and Jurassic). Also note prehistoric petroglyphs on some of the fracture surfaces.

FIGURE 13. Fracture-surface structures on a fracture face at Stop 4-1. Hammer in crack for scale.

DAY 4 STOP 2
DEFORMATION BANDS AT VALLEY OF FIRE STATE PARK
(Geologic map, Bohannon, 1983)

Here we will examine a network of deformation bands exposed in a natural pavement of the Aztec Sandstone. Mr. Robin Hill of the Geology Department at the University of Nevada, Las Vegas, is mapping and characterizing the bands exposed on the pavement for his master's thesis. His preliminary map is shown on figure 14. These bands are quite different from the fractures observed so far on this trip. Thin-section examination of the bands reveals them to be zones of reduced porosity, which makes them more resistant to weathering so that they stand out in positive relief on the pavement surface. As viewed in thin section, the bands exhibit no evidence of crushing or reduction in grain size relative to the rock matrix outside the bands, both of which are described for deformation bands by Aydin (1978) and Aydin and Johnson (1978). A few exhibit small shear displacement on the order of millimeters to a centimeter across the bands. Some of the grain-to-grain contacts in the bands are concavo-convex, suggesting pressure solution. The bands occur in swarms. There are three sets of bands, one of which is crenulated along both the strike and dip directions. Study of the traces of individual deformation bands on the outer edges of the swarms reveals that they often curve off into the directions of the other two sets. We have no explanation for this behavior. These bands have acted as both conduits and barriers to fluid flow as can be seen by the patterns of iron oxide staining by groundwater.

DAY 5 STOPS 1 and 2
FRACTURE NETWORKS AT YUCCA MOUNTAIN, NEVADA
(Geologic map, Scott and Bonk, 1984)

Fracture studies are part of the U.S. Geological Survey's effort to characterize the geologic and hydrologic framework at Yucca Mountain, Nevada. The site is currently being evaluated by the U.S. Department of Energy as a potential underground repository for high-level radioactive waste.

The impetus for this study is three-fold:
(1) Hydrologic flow through fracture networks is a means by which water could reach buried radioactive waste and transport radionuclides out of the repository. Open networks are the primary avenues of rapid transport for liquids and gases through rock masses. In contrast to fracture-network flow, rock-matrix flow generally is significant only for slow transport rates. Measured network permeabilities are six to seven orders of magnitude greater than matrix permeabilities (Montazer and Wilson, 1984). Precipitation of minerals from aqueous solutions along fractures indicates that in the geologic past, water has moved through Yucca Mountain along fractures.

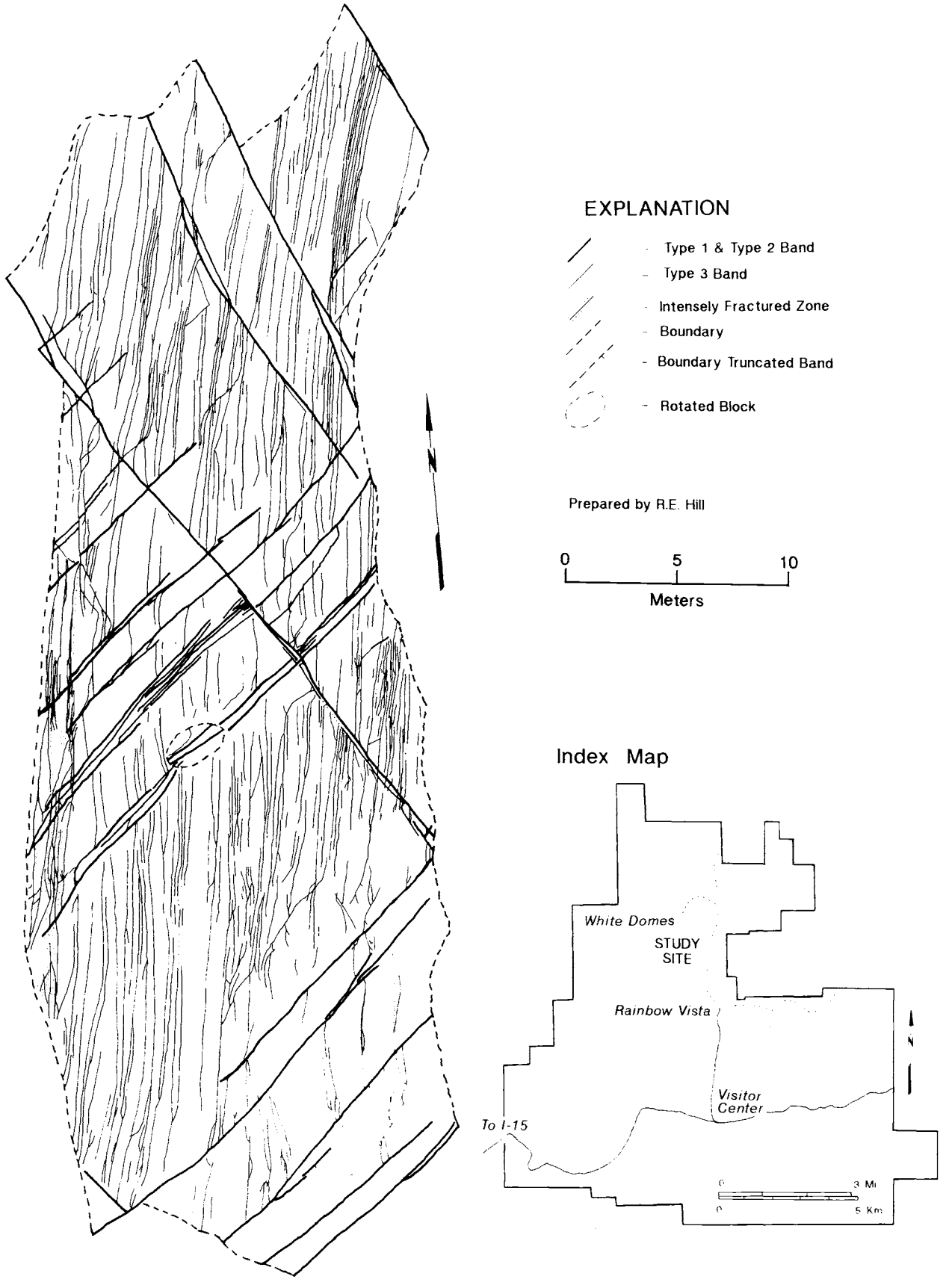

FIGURE 14. Traces of deformation bands, Stop 4-1, Valley of Fire State Park, Nevada.

(2) Because Yucca Mountain is composed of large and small fracture-bounded blocks, the mechanical stability of the mountain during and after the construction of an underground repository depends in part on the geometry of the fracture networks. (3) The fracture network is a composite of sequential fracture formation and reactivation events (Barton and others, 1986), which record parts of the paleostress history of the mountain.

Characterization of fractures for fluid-flow, geomechanical, and paleostress models now in use or under development cannot be achieved by the standard methods of study. Standard methods, such as those outlined in Kulander and others (1979), are based only on sampling natural outcrops and cores and do not include mapping of the fracture traces. While outcrop and core studies permit characterization of orientation, aperture, mineralization, and surface roughness, they do not permit characterization of trace length, spatial distribution, interconnectivity, or the size and shape of fracture-bounded blocks, all of which can be measured from a fracture-trace map of a pavement surface. All of the characteristics listed above are necessary for fluid-flow and geomechanical modeling. The pavements are two-dimensional sections through three-dimensional fracture networks. Three perpendicular pavements are necessary to completely sample three-dimensional fracture networks.

Maps of fracture traces that adequately sample a fracture network are rare;. the only such published maps that we are aware of are contained in three papers. Segall and Pollard (1983a and 1983b) mapped fracture traces on glacial pavements in the Mount Givens Granodiorite in the Sierra Nevada of California. La Pointe and Hudson (1985) mapped fractures on a quarry floor in the Niagara Dolomite at Lannon, Wisconsin. All other published maps that we are aware of do not adequately sample the fracture network because one dimension of the map is too small (for example, mine-wall maps), or because the range in fracture trace length mapped was too small. An optimal map would cover an area large enough to include both ends of the longest fracture exposed. Our own maps only approach this optimal size. Therefore, in order to adequately sample the fracture network, we have mapped all fractures from the longest down to an arbitrarily chosen value of 0.2 m.

Contemporary fluid-flow and geomechanical models are generalized and use simulated networks (Long, 1983; Robinson, 1984; Long and others, 1985; Goodman and Shi, 1985; Lemos and others, 1985). Site-specific models require site-specific fracture parameters. The method of pavement studies described below is the best basis for complete characterization; it characterizes and integrates the nine fracture parameters discussed above. Published fluid-flow and geomechanical models are too primitive to incorporate all of the parameters. The relevance of the parameters has been discussed above, and assures their incorporation in more sophisticated future models.

At Stop 1, we will visit three pavement sites mapped near drill hole USW G-4. The exposed bedrock pavements are designated 100, 200, and 300. Pavement 100 is on Live Yucca Ridge 500 m south of pavements 200 and 300, which are 15 m apart on Dead Yucca Ridge. All three pavements are in the densely welded, upper lithophysal unit of the Tiva Canyon Member of the Miocene Paintbrush Tuff. At Stop 2 we will visit pavement 1000, located in the densely welded orange brick unit of the Topopah Spring Member of the Miocene Paintbrush Tuff.

Fracture Network Maps

The map bases used for mapping the pavements were aerial photographs taken from a helicopter at an altitude of approximately 150 m. The orientation and scale of the bases were determined directly from 2-m-long, 0.22-m-wide arrows placed on the pavements and oriented to true north. Where the aerial photograph was not normal to a pavement surface, the maps were rectified by removing distortion of the arrows.

We mapped directly on the pavements, adding fractures not visible on the photographs. All fractures more than 0.2 m long were mapped on clear acetate sheets laid over the aerial photo bases. Attention to fracture intersections, abutments, and offset relationships was emphasized.

The pavement surfaces are not excessively weathered because they were protected by overlying debris until exposed for study. Shallow dipping, bowl-shaped fractures and fractures of limited vertical extent were considered to be due to weathering and were not mapped or studied.

Figures 15, 16, 17, and 18 are maps of the three pavements at Stop 1 and the one pavement at Stop 2.

Comparison of Methods for Studying Fractures

The standard geologic methods for characterizing fractures use outcrops, boreholes and cores, and aerial photographs. Outcrops permit measurement of orientation, roughness, mineralization, aperture, abutting relations, and tectonic features. Normally, however, there is little choice where to measure these characteristics because only a very small portion of each fracture is exposed. It is not usually possible to determine the trace length, spatial distribution of traces and their intersections, and connectivity, or the sizes, shapes, and geometries of blocks bounded by fractures. These are characteristics of the network that are necessary for hydrologic and geomechanical modeling.

Boreholes and cores together permit measurement of orientation, roughness, mineralization, aperture, and tectonic features, but

these characteristics may not be representative because only a very small portion of the fracture is recovered or exposed in the borehole wall. It is impossible to determine trace length, spatial distribution of traces and intersections, connectivity, abutting relations, or the size, shape, and spatial distribution of blocks bounded by fractures. The primary limitation of boreholes and cores is that they are a one-dimensional sampling of a three-dimensional fracture network. Moreover, vertical holes and cores are normally subparallel to the dip of most of the fractures, and therefore provide a limited and biased sampling of fractures that can not be corrected by statistical analysis.

Studies of fractures from aerial photographs have proven to be extremely limited. At best they provide strike (but not dip) and spatial patterns and densities. At Yucca Mountain they can not even provide these characteristics; linear features on the photographs have been shown not to correspond to fractures on the ground (Throckmorton, 1987).

The pavement method permits the most accurate and complete sampling of the individual and network characteristics of fractures. A comprehensive study requires pavements in three perpendicular planes. The size of all of these pavements falls short of revealing a characteristic, representative elementary area of the fracture pattern. A larger pavement, 1720 m^2 in area in the same upper-lithophysal unit of the Tiva Canyon Member exposed on top of Busted Butte, 9 km to the south and mapped subsequent to this study, also does not reveal a representative elementary area of the fracture pattern, implying either that prohibitively large pavements are required or that there is no representative elementary area for the fracture pattern in this unit. The fractal behavior of fracture and fault-trace patterns discussed above suggests that they are self-similar over a broad range of scales at Yucca Mountain. For a fractal object, any part is statistically the same as the whole object. Thus, for three-dimensional patterns of fractures that are fractal, the concept of a representative elementary volume applies. Therefore, fractal geometry of the fracture-trace patterns is useful for extrapolating both upward and downward in size from the necessarily limited size of the pavements.

Pavements at the ground surface are subject to weathering and stress release due to unloading. Underground, they are subject to the stress redistribution present around all underground surfaces. Nevertheless, we conclude that the pavement method is at present the best method for characterizing fractures and fracture networks for hydrologic, geomechanical, and paleostress modeling.

DAY 5 STOP 3
GAS-FLOW IN WELLS AT THE CREST OF YUCCA MOUNTAIN

(Geologic maps, Scott and Bonk, 1984; Maldonado, 1985)

Two wells were drilled at the crest of Yucca Mountain to provide access for measurement of rock moisture and rock gas chemistry. USW UZ-6 was drilled to a depth of 575 m and cased to a depth of 99 m, below which the well was left open. Well USW UZ-6S was drilled to a depth of 158 m and had a one-meter surface casing. Both wells were completed in thick sections of unsaturated fractured tuffs. The water table at the well site is approximately 710 m below land surface.

Substantial airflow has been observed in both wells (Weeks, 1987). During winter, the wells exhaust air into the atmosphere at a velocity of about 3 m/s. The exhaust air has a temperature of about 18°C and is saturated with water vapor. Weeks calculated that, during winter, UZ-6 discharges about 560 L of water a day into the atmosphere, while UZ-6S discharges about 125 L a day. During summer, the wells alternately intake and exhaust air. The flow direction reverses at least a few times a day, and flow velocity is much lower than during winter. Taken together, the summer and winter observations suggest that there is a natural air circulation through the unsaturated zone at Yucca Mountain. This possibility is supported by computer simulations conducted by Kipp (1987).

Weeks (1987) suggested two mechanisms to explain the air flow: a topographic effect and a barometric effect. From the crest of Yucca Mountain, the land surface drops about 250 m down a steep western scarp to the Solitario Canyon floor. During the winter, a column of air extending from the altitude of the mountain crest down to a rock outcrop on the mountain scarp will be cooler, drier, and therefore denser than the equivalent column of warm, moist air in the well. Thus, air will enter the outcrop on the mountain scarp, flow through the fractured tuff to the well, and exit the well at the mountain crest. During the summer, the conditions should be reversed and the well should take in air.

The barometric effect arises from the difference in transmission time needed for a change in barometric pressure at the land surface to be propagated underground. Two pathways are available for pressure propagation: down the well bore and through the unsaturated zone. While the propagation down the well bore is almost instantaneous, the propagation through the unsaturated zone is considerably slower. This leads to an imbalance between the pressure in the wellbore and the pressure in the fractured rock of the unsaturated zone. During periods of rising barometric pressure, air will flow from the well into the rock (i.e., the well will take in air), while during periods of falling barometric pressure, air will flow from the rock to the well (i.e., the well will exhaust air).

The airflow in wells UZ-6 and UZ-6S is probably caused by a combination of the topographic and barometric effects. Weeks (1987) noted that these effects can adequately explain the frequent reversals of airflow during the summer, but

FIGURE 15. Fracture-trace map of pavement 100, Stop 5-1, Yucca Mountain, Nevada.

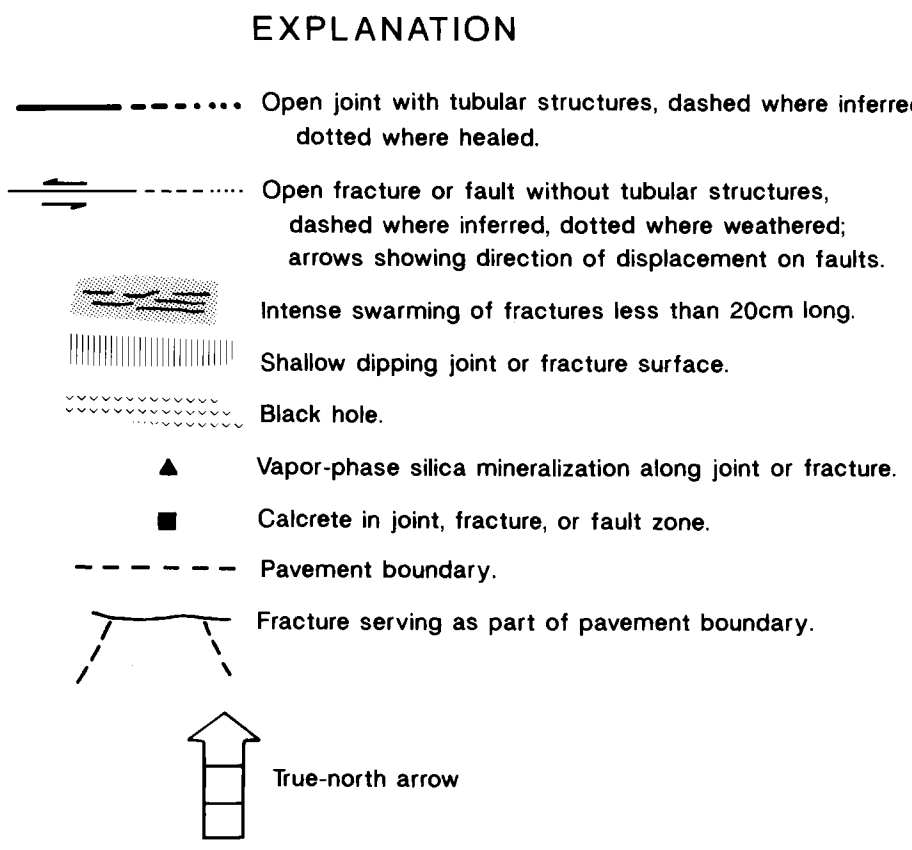

FIGURE 15. Continued

are insufficient to account for the much greater air exhaust during the winter. Studies are currently underway to examine other mechanisms that may act as driving forces of air flow in boreholes opened to the unsaturated zone.

PART III - ROAD LOG

Day 1

0 km (0 mi) Intersection of Interstate 15 and U.S. Rte. 95 Las Vegas, Nevada.

Drive north on I-15. To the southwest (back to the left) are the Spring Mountains. To the northwest (ahead) is the south end of the Las Vegas Range. To the east (right) is Frenchman Mountain. Continue north through the Dry Lake Range with the Las Vegas Range on the west (left).

34.6 km (21.5 mi) Exit onto U.S. Rte. 93. Drive through the underpass and stop. To the west (ahead) is the Las Vegas Range. To the north-northwest (ahead and to the right) is the Arrow Canyon Range. To the north (right) are the Meadow Valley Mountains. Continue west through the southern end of the Arrow Canyon range and continue north along Hidden Valley and Coyote Spring Valley. To the west (left) is the Las Vegas Range, to the east (right) is the Arrow Canyon Range.

92.2 km (57.3 mi) Turn east (right) onto Nevada State Rte. 168. To the south (right) is the north end of the Arrow Canyon Range. To the east (ahead) is the Muddy River Valley. To the north (left) are the Meadow Valley Mountains.

100.4 km (62.4 mi) Pull off on north side of road and park. Walk 1.6 km north up Wildcat Wash. **STOP 1.** Drive east on Nevada State Rte. 168.

105.2 km (65.4 mi) Turn sharp right onto paved road into Warm Springs Oasis. The springs discharge here because of the intersection of the ground water potentiometric surface and a topographic low.

109.3 km (67.9 mi) Turn left into the Taylor Ranch. **STOP 2.**
(Note: This stop is on private property - no trespassing without permission of the owner.)

111.8 km (69.5 mi) Cross Muddy River. Note U.S. Geological Survey gaging station up stream to left of road. Flow rate is constant year round, indicating a large groundwater reservoir feeding the springs that in turn feed the Muddy River.

113.3 km (70.4 mi) Turn east (right) back onto Rte. 168 and continue east.

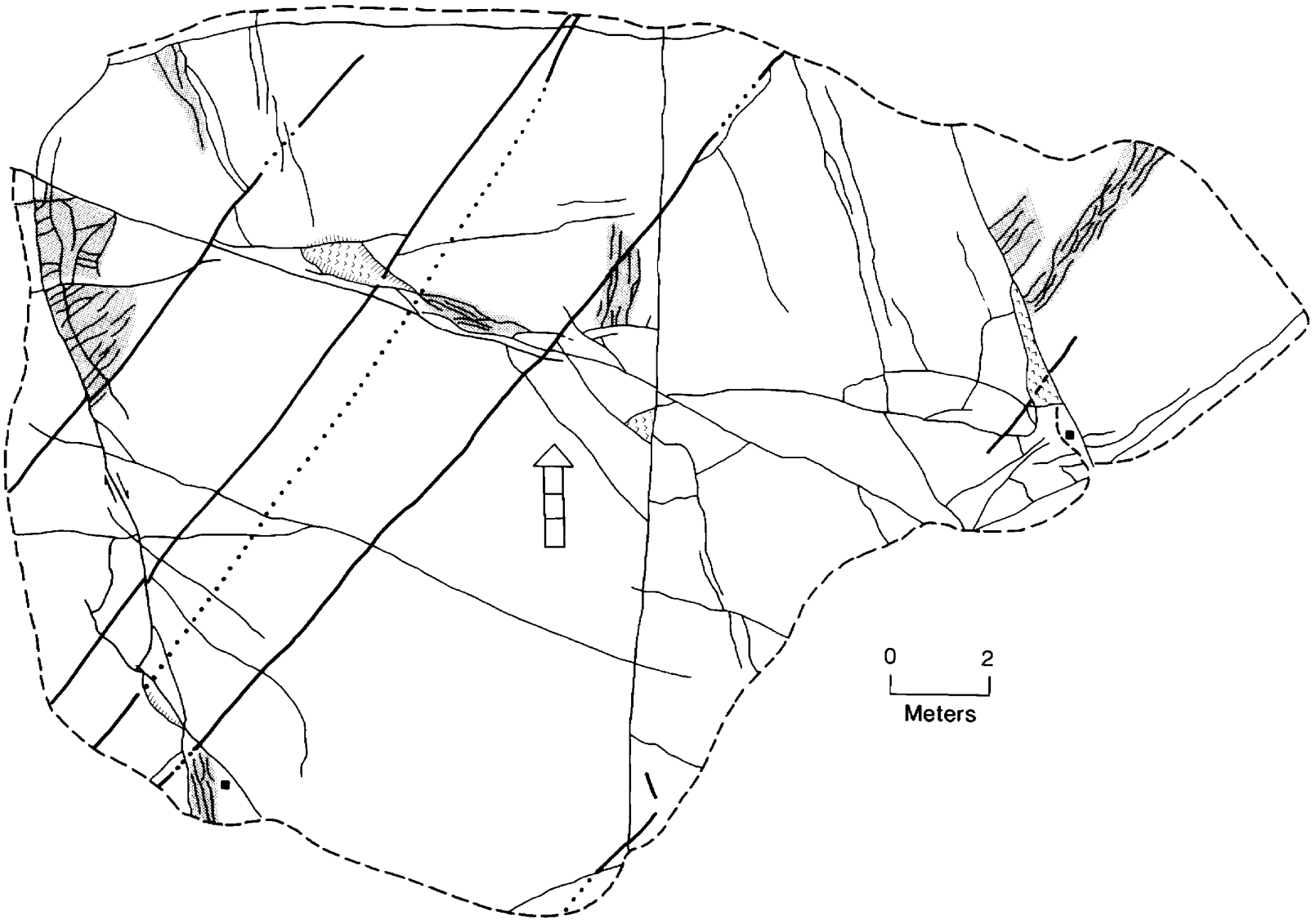

FIGURE 16. Fracture-trace map of pavement 200, Stop 5-1, Yucca Mountain, Nevada. (Explanation shown on fig. 15)

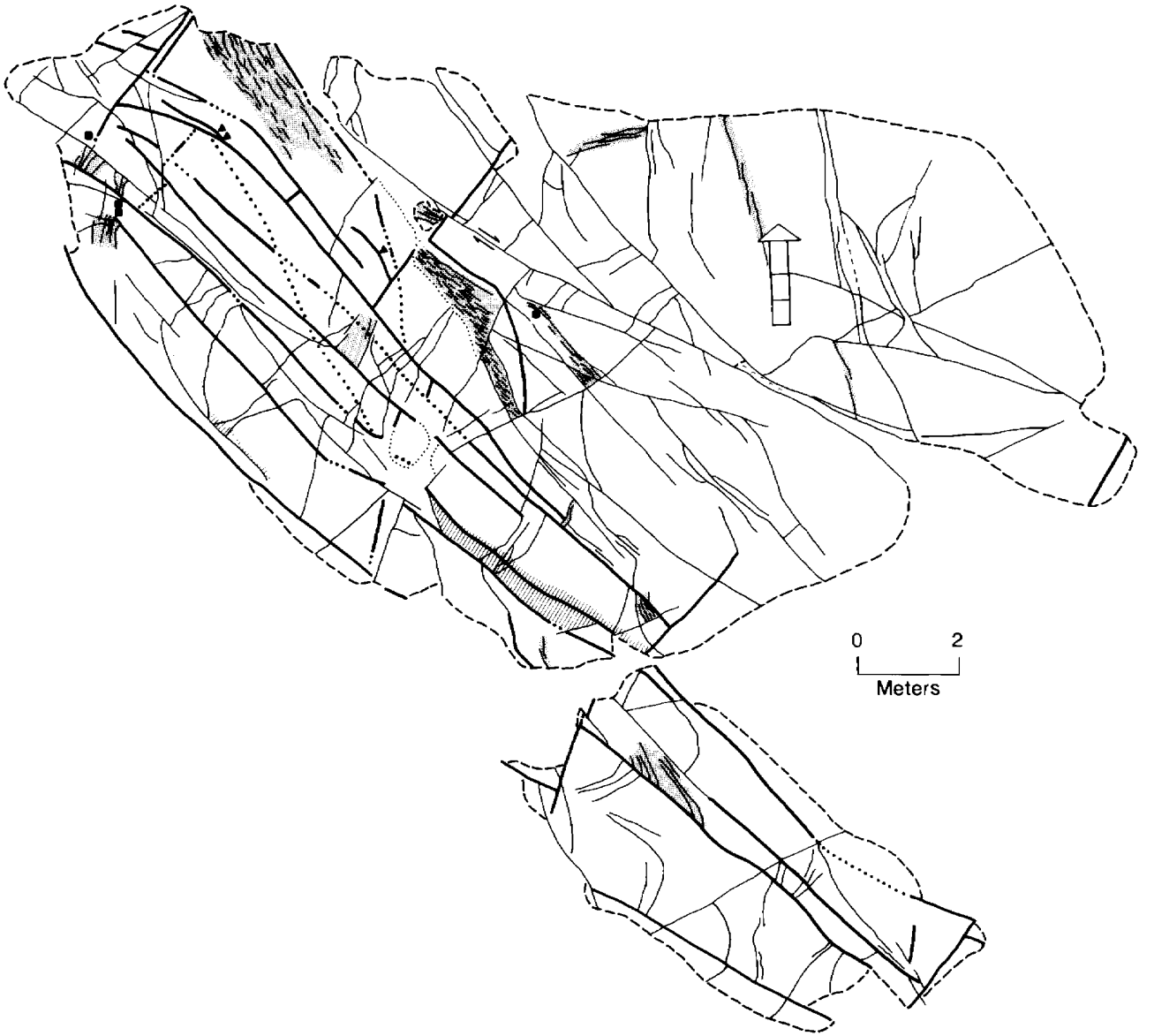

FIGURE 17. Fracture-trace map of pavement 300, Stop 5-1, Yucca Mountain, Nevada. (Explanation shown on fig. 15)

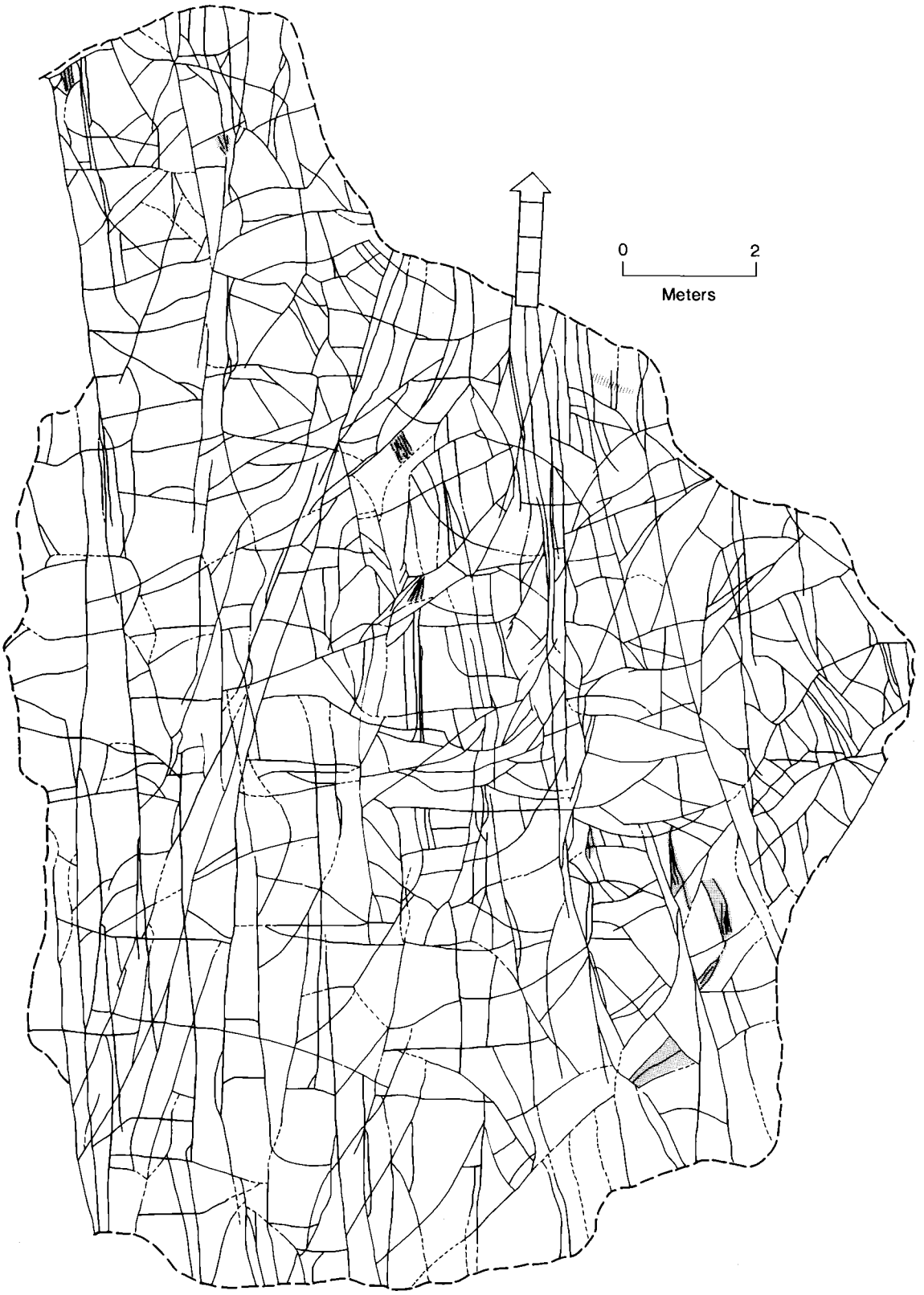

FIGURE 18. Fracture-trace map of pavement 1000, Stop 5-2, Yucca Mountain, Nevada. (Explanation shown on fig. 15)

124.5 km (77.4 mi) Cross Muddy River at Town of Glendale and follow signs through construction area to I-15 north.

126.0 km (78.3 mi) Junction of Rte. 168 and I-15 north. Northbound on I-15, we drive northeast along the top of Mormon Mesa and Flat Top Mesa. To the south (back to the right) are the Muddy Mountains. To the east (ahead to the right) are the Virgin Mountains. To the north (left) are the Mormon Mountains.

158.5 km (98.5 mi) Begin descent into the Virgin River Valley.

177.5 km (110.3 mi) Arizona State line. To east (right) are the Virgin Mountains.

192.3 km (119.5 mi) Cross Virgin River.

197.9 km (123.0 mi) Enter Virgin River Gorge. This 762-m-deep canyon exhibits the best exposures of Paleozoic sedimentary rocks in southwestern Utah. Both the Virgin Mountains to the south and the Beaver Dam Mountains to the north are cored by Precambrian crystalline rocks. The Paleozoic section consists of about 494 m of Cambrian quartzite, shale and dolomite; 143 m of Devonian dolomite; 189 m of Mississipian Redwall Limestone; 213 m of Pennsylvanian limestone and sandstone; and about 671 m of Permian rocks including the Pakoon Limestone, the thick Queantoweap Sandstone, and carbonate and evaporite units of the Toroweap Formation and Kaibab Limestone. Structures include thrust faults (both older-on-younger and attenuation), reverse and tear faults, and extension faults, all of post-Paleozoic (post Jurassic?) ages (Steed, 1980; Hintze, 1980). Note that most fractures are stratabound within individual subunits or groups of subunits.

198.4 km (123.3 mi) Mississippian Redwall Limestone.

200.0 km (124.3 mi) Devonian light-colored dolomite uncomformably overlying Cambrian carbonate rocks.

201.6 km (125.3 mi) Cambrian Bonanza King Formation carbonate rocks with numerous solution cavities.

204.0 km (126.8 mi) Massive cliffs of Cambrian, Devonian, and Mississippian rocks to north (right). Cross Cedar Pockets Wash fault with upper Paleozoic rocks on downthrown (east) side against Mississippian Redwall Limestone.

205.6 km (127.8 mi) Queantoweap Sandstone (red) cut by small faults.

208.8 km (129.8 mi) Cross the large extensional Grand Wash fault with west side downdropped. Displacement here is about 366 m but south in Arizona, displacement increases to at least 1219 m and may be as much as 4877 m.

212.9 km (132.3 mi) Queantoweap Sandstone.

216.1 km (134.3 mi) Excellent exposures of Permian Queantoweap Sandstone, Toroweap Formation, and Kaibab Limestone.

219.3 km (136.3 mi) Toroweap Formation and Kaibab Limestone.

224.6 km (139.6 mi) Arizona - Utah state line. Kaibab Limestone and lower units of the Moenkopi Formation (Triassic). Town of St. George, Utah is 8 km ahead. To the north beyond St. George are the Pine Valley Mountains, cliffs of Navajo Sandstone (Triassic? and Jurassic), overlain by Jurassic, Cretaceous, and Tertiary sedimentary rocks and capped by 914 m of monzonitic rocks of the Pine Valley laccolith (mid-Tertiary) which covers 181 km^2.

Note time zone change; set watches ahead 1 hr.

248.1 km (154.2 mi) Columnar joints are well developed in Cenozoic basalt flow in roadcut. Late Cenozoic basalt flows range in age from about 2 Ma to perhaps less than a few thousand years. Four major stages of intrusion are recognized in the region. Mineralogical composition and the presence of peridotite xenoliths suggest deep sources with control by deep extensional fractures.

249.9 km (155.3 mi) Exit onto Utah State Rte. 9 east. Pass through Navajo Sandstone (Triassic? and Jurassic) capped by late Cenozoic basalt flows exhibiting columnar jointing and multiple cooling units.

250.7 km (155.8 mi) Pass through west limb of the northeast-trending, erosionally breached, Virgin anticline in the Moenkopi Formation.

255.8 km (159.0 mi) Cross Virgin River.

265.8 km (165.2 mi) Rte. 9 turns north in the town of Hurricane, Utah, and runs parallel to the Hurricane Cliffs to the east (right). The trace of the Hurricane fault, a main Basin and Range style normal fault with approximately 2438 m of dip slip and offset down to the west near Hurricane, runs parallel to Rte. 9 along the base of the Hurricane Cliffs. Maximum displacement on the fault may be as much as 3000 m. The cliffs (upthrown side) here consist of limestones of the Toroweap and Kaibab (Permian) capped by basal Moenkopi Formation (Triassic).

267.4 km (166.2 mi) Cross the Virgin River at bridge. To the east (right), the trace of the Hurricane fault is visible at the canyon mouth, with Triassic Chinle and Moenkopi Formations on the downthrown (west) block against Toroweap Formation and Kaibab Limestone (Permian). The Pah Tempe hot springs issue from the limestone of the Toroweap at and near river level.

269.7 km (167.6 mi) Intersection of Rte. 9 loop and Rte. 9 east, turn right and continue on Rte. 9 east towards the Hurricane Cliffs.

271.9 km (169.0 mi) Exposure of steeply dipping slickensided surface in the Hurricane fault zone to the south (right). This is the surface of a subsidiary fault. The main displacement is approximately 0.8 km to the west.

275.9 km (171.5 mi) Driving east on Rte. 9 in Moenkopi Formation (Triassic). To the northeast (ahead and left) are cliffs of Moenkopi capped by the Shinarump Member of the Chinle Formation (Triassic). To the east (ahead) are cliffs of Moenkopi capped by a Quaternary basalt flow. To the southeast (ahead and right) buttes and mesas of

Moenkopi are capped by the Shinarump. The low regional dip is east-northeast so that the route slowly ascends the stratigraphic section.

283.3 km (176.1 mi) Quaternary basalt flow exhibiting poorly developed columnar joints in road cut on north side of road (left). Continue east on Rte. 9 through towns of Rockville and Springdale, Utah. The Shinarump Member and the overlying Petrified Forest Member of the Chinle Formation are exposed at road level on the outskirts of Springdale, Utah.

302.3 km (187.9 mi) Entrance to Zion National Park. Ahead are spectacular views of the Navajo Sandstone (Triassic? and Jurassic) cliffs underlain by the red beds of the Kayenta and Moenave Formations (Upper Triassic?). The Navajo Sandstone exhibits a tripartite color division that does not correspond to bedding and is probably caused by oxidation-reduction associated with paleogroundwater systems. The upper third is white, the middle third is pink, and the lower third is gray and brown. This is also the type area of the 30.5-m-thick cliff-forming pinkish Springdale Sandstone Member of the Moenave which crops out about 150 m below the Navajo.

303.6 km (188.7 mi) Turn north (left) into Visitor Center. The group will receive an hour-long lecture and film on the geology and ecology of Zion National Park. Maps, books, and postcards are for sale here.

304.6 km (189.3 mi) Turn north (left) at intersection onto Floor of the Valley Road along the north fork of the Virgin River, after crossing bridge.

305.9 km (190.1 mi) Stop at pulloff on east side of road (right). Water seepage on cliff of Moenave Formation 15 m above North Fork of the Virgin River to the west across the road. The white seepage stains are salts forming by evaporation of the water as it emerges from subhorizontal bedding-plane fractures.

307.3 km (191.0 mi) Court of the Three Patriarchs to the west (left).

309.0 km (192.1 mi) Turn east (right) into parking area for Zion Lodge. End of road log for Day 1.

Day 2

0 km (0 mi) Leave Zion Lodge parking lot, turn north (left) onto Floor of the Valley Road.

1.3 km (0.8 mi) Angel's Landing to north (ahead).

4.2 km (2.6 mi) Turn east (right) into the Weeping Rock parking area. Walk along path across footbridge above discharge from Weeping Rock and follow signs 0.40 km miles up grotto to Weeping Rock.

STOP 1. Weeping Rock.

Leave parking area, turn south (left) onto Floor of the Valley Road.

8.4 km (5.2 mi) Zion Lodge to east (left).

12.9 km (8.0 mi) Turn west (right) at intersection onto Rte. 9.

15.1 km (9.4 mi) Leave Zion National Park and pass through Springdale travelling south and west toward Rockville.

22.4 km (13.9 mi) Turn sharp right onto unpaved access road to Rockville cemetery. Park on flat ground (do not block access to cemetery).

STOP 2

22.4 km (13.9 mi) Leave through cemetery. Turn east (left) onto Rte. 9.

29.6 km (18.4 mi) Enter Zion National Park.

31.9 km (19.8 mi) Turn north (left) at intersection onto Floor of the Valley Road.

36.4 km (22.6 mi) Zion Lodge, turn east (right) into parking lot. End of road log for Day 2. Lecture after dinner.

Day 3

0 km (0 mi) Leave Zion Lodge parking area, turn south (left) onto Floor of the Valley Road.

4.5 km (2.8 mi) At intersection, turn east (left) onto Rte. 9 up Pine Creek Canyon. Note steeply dipping stratabound fractures and bedding-plane partings in the subunits of the Moenave and the overlying Kayenta Formations (Upper Triassic?).

8.7 km (5.4 mi) Observe Great Arch of Zion to the east (ahead) in the basal Navajo Sandstone. The arch is formed by convex-upward fractures that abut against (and are therefore younger than) the subvertical release fracture framed by the arch.

10.0 km (6.2 mi) Rte. 9 enters first tunnel.

11.7 km (7.3 mi) Exit tunnel. Note excellent exposure of large festoon cross-beds mostly dipping SSW in the Navajo Sandstone formed by southward sand dune advance in Triassic? and Early Jurassic time.

12.7 km (7.9 mi) In cliff to south (right) note swarm of N10°-20°W subvertical fractures with vertical exposure of more than 90 m in the Navajo Sandstone.

13.8 km (8.6 mi) Rte. 9. enters second tunnel.

14.5 km (9.0 mi) **STOP 1.**

Continue driving east on Rte. 9. Note that the topography along the roadside is shaped by the festoon cross-beds in the Navajo Sandstone. Note that between the swarms of subvertical fractures, the dominant fractures are the subhorizontal partings between the cross-bed sets.

19.8 km (12.3 mi) Cross onto north side of Rte. 9 and park at Checkerboard Mesa view point pull-off. **STOP 2.**

Continue to drive east.

21.2 km (65 mi) Leave Zion National Park and continue east on Rte. 9.

Continue east up section sequentially through the Navajo Sandstone, Temple Cap Sandstone (Jurassic), Carmel Formation (Jurassic), and Tropic Shale (Cretaceous) then down section into the middle part of the Carmel Formation as you continue east toward Mt. Carmel Junction. To the east (ahead) see in the distance the Elkhart Cliffs

(white) and to the ESE (ahead, right) Meek's Cliffs at the northern end of Block Mesa. Both cliffs are expressions of the upper white unit of the Navajo Sandstone capped by the Temple Cap Sandstone and the Carmel Formation.

40.2 km (25.0 mi) Descend into the valley of the headwaters of the East Fork of the Virgin River.

41.2 km (25.6 mi) Mt. Carmel Junction. Turn south (right) onto U.S. Rte. 89.

45.5 km (28.3 mi) Cross the trace of the Sevier fault. A single clean fault plane is not visible, but the roadcut exposes shattered Carmel Formation. The Sevier fault is a regional NNE- striking, steeply west-dipping normal fault with offset ranging from 30-300 m down to the west.

46.7 km (29.0 mi) To west (right) is the road to Coral Pink Sand Dunes State Park. Continue southeast on Rte. 89 driving on top of the Wygaret Terrace. The White Cliffs of Navajo Sandstone capped by the Temple Cap Sandstone and Carmel Formation are off to the east (left).

56.8 km (35.3 mi) Road descends into the Kanab Creek Valley, sequentially through the Navajo Sandstone, Kayenta Formation, and Moenave Formation, to the Chinle Formation.

57.4 km (35.7 mi) Kanab Canyon extends to the north along Kanab Creek.

58.4 km (36.3 mi) Cross over Kanab Creek.

61.3 km (38.1 mi) Drop down through the Vermillion Cliffs of Kayenta Formation.

63.7 km (39.6 mi) Enter town of Kanab, Utah.

65.8 km (40.9 mi) Intersection. Continue south (straight ahead) on U.S. Rte. Alt. 89 to Fredonia, Arizona.

70.0 km (43.5 mi) Stop at pull-off at Fort Kanab historic sign post on west side of road and view Vermillion Cliffs in the distance to the west.

70.6 km (43.9 mi) Arizona State Line. Note time zone change; set watches back one hour.

71.0 km (44.1 mi) Enter Fredonia, Arizona.

76.7 km (47.7 mi) Intersection with Arizona State Rte. 389. Continue south (straight ahead) on Rte. Alt. 89 toward Jacob's Lake. We are driving on top of the Kanab Plateau and the Kaibab monocline; to the north (left) are the Vermillion Cliffs and the White Cliffs. The Kaibab Plateau is ahead on the skyline.

102.0 km (63.4 mi) Enter Kaibab National Forest. Continue driving up onto top of the Kaibab Plateau. Exposures of the Kaibab Limestone and the Toroweap Formation (Permian) in roadcuts as we drive up onto the top of the Kaibab Plateau.

106.7 km (66.3 mi) Turn east (left) into parking area at scenic view point. Walk up path 0.16 km to observation shelter. On a clear day this is a 150-km view to the NW of the Vermillion Cliffs (Kayenta), White Cliffs (Navajo), Grey Cliffs (Cretaceous Straight Cliffs Formation), and Pink Cliffs (Tertiary Wasatch or Claron Formation), each progressively higher in the stratigraphic section and farther away from this vantage point. Together the steps of the cliffs are called the grand staircase.

124.5 km (77.4 mi) Intersection of Rtes. Alt. 89 and 67 at Jacob's Lake, Utah. Continue south (straight ahead) on Rte. 67.

166.0 km (103.2 mi) Entrance to Kaibab Lodge to east (left).

175.2 km (108.9 mi) Entrance to Grand Canyon National Park

190.8 km (118.6 mi) Intersection. Turn east (left) onto road to Cape Royal and Point Imperial.

199.7 km (124.1 mi) Intersection. Turn south (right) onto road to Cape Royal.

222.8 km (138.5 mi) Arrive at parking area for Cape Royal.

STOP 3.

Leave Cape Royal and retrace route to Rte. 67.

223.8 km (139.1 mi) Pulloff on east (right) side of road. Walk 32 m to roadcut ahead.

STOP 4.

Retrace route to Rte. 67 (31 km).

254.9 km (158.4 mi) Intersection with Rte. 67. Turn south (left) onto Rte. 67.

259.7 km (161.4 mi) Turn east (left) into parking area for the North Rim Lodge.

STOP 5.

End of road log for day 3.

Day 4

0 km (0 mi) Retrace route of Day 3 from North Rim Lodge through Zion Park (without turning off Rte. 67 to Cape Royal) and of Day 1 from Zion Park toward Las Vegas.

316.8 km (196.9 mi) Cross state line into Nevada.

391.0 km (243.0 mi) Exit from I-15 onto Nevada State Rte. 169 east to the Valley of Fire in the North Muddy Mountains.

398.1 km (247.4 mi) To the northeast (ahead left) are the North Muddy Mountains. To the southeast (ahead right) are the Muddy Mountains.

403.6 km (250.8 mi) Enter the Muddy Mountains.

411.6 km (255.8 mi) Exposed in hill to north (left) of road is Moenave Formation (Upper Triassic?).

413.9 km (257.2 mi) Enter Valley of Fire State Park.

414.2 km (257.4 mi) Stunning exposures of the Aztec Sandstone (Triassic? and Jurassic) to the northeast (ahead and left).

420.1 km (261.1 mi) Turn north (left) into Visitor Center parking lot. At the center we will have a short presentation on the geology of the park. Leave the Visitor Center and drive along the unnamed paved road through the small canyon to the west and north of the Visitor Center.

422.5 km (262.5 mi) Pull off road into parking area for Mouse's Tank on the east (right) side of road. **STOP 1.** Continue driving north.

423.7 km (263.3 mi) Rainbow Vista. Park vehicle and walk 2.5 km along the dirt road that continues north from the end of the paved road,

toward the White Domes area. At 2.5 km, look for large tree approximately 61 m to the west of the unpaved road.
The tree marks the location of **STOP 2.**
Return to the vehicle and retrace route to I-15.

456.3 km (283.5 mi) Intersection of Rte. 169 and I-15. Go south on I-15 to Las Vegas.

508.8 km (316.2 mi) Intersection. Exit onto U.S. Rte. 95 west. Drive NW on Rte. 95 along the trace of the Las Vegas shear zone, a right-lateral regional structure. To the west (ahead) are the Spring Mountains. To the north (right) is the Las Vegas Range.

527.9 km (328.0 mi) To the south (left) in the Spring Mountains the Keystone thrust separates the white peaks and cliffs of the Goodsprings Dolomite (Cambrian-Devonian?) from the Aztec Sandstone (Triassic? and Jurassic) below.

535.7 km (332.9 mi) Intersection. Turn south (left) onto Nevada State Rte. 157. Proceed south along the top of the alluvial fan of the Spring Mountains.

550.9 km (342.3 mi) Enter wash cut down into the alluvial fan.

562.8 km (349.7 mi) Turn east (left) into parking area for the Mount Charleston Hotel. End of road log for Day 4. Discussion forum and presentations by field trip participants before and after dinner.

Day 5

0 km (0 mi) Leave Mt. Charleston Hotel parking area and turn south (left) onto Rte. 157.

1.0 km (0.6 mi) Intersection. Turn west (right) onto Nevada State Rte. 158. Enter Toiyabe National Forest.

2.7 km (1.7 mi) Astronomical Observatory to the northwest (ahead) on ridge at skyline.

12.9 km (8.0 mi) Panorama to the north (right) across the Las Vegas shear zone. From west to east are the southern ends of the north-trending Pintwater Range, Desert Range, and Sheep Range.

15.1 km (9.4 mi) Intersection. Turn north (right) onto Nevada State Rte. 156 and proceed down the surface of the alluvial fan to the Las Vegas Valley floor.

37.8 km (23.5 mi) Intersection. Turn west (left) onto U.S. Rte. 95. To the NNW (ahead right) is the Pintwater Range. To the NW (ahead) is the Spotted Range at the skyline.

58.9 km (36.6 mi) Village of Indian Springs, Nevada. The springs are located on private property approximately 1.6 km south of Rte. 95. The Spring Mountains are the most likely source region for the springs, which are forced to the surface, perhaps by encountering an impermeable Las Vegas shear zone.

60.0 km (37.3 mi) Entrance to U.S. Air Force base to north (right). Home base of the Thunderbirds, a jet-fighter unit specializing in precision flying and aerobatics.

64.0 km (39.8 mi) Oasis of Cactus Springs, Nevada.

81.0 km (50.3 mi) Nye County line.

88.8 km (55.2 mi) Exit north (right) and proceed along Mercury Highway to the entrance of the Nevada Test Site. To the NE (right) is the Spotted Range. To the north (ahead) is Red Mountain, behind Mercury. To the NNW (ahead left) is Skull Mountain. To the NW (ahead left) is Little Skull Mountain. To the west (left) is the Spector Range.

94.4 km (58.7 mi) Entrance to the Nevada Test Site. Turn east (right) into parking area and proceed into the Badge Office. (Note: cameras and binoculars cannot be brought onto the Nevada Test Site. They can be deposited at the Badge Office and picked up again when you leave). Reboard vehicle and proceed north through the gate.

95.9 km (59.6 mi) Intersection. Turn west (left) onto Jackass Flat Road and proceed west. Spector Range to the west ahead.

103.1 km (64.1 mi) Intersection. Bear right and continue on Jackass Flat Road.

108.6 km (67.5 mi) Skull Mountain to NW (ahead right) of Tertiary volcanics (pink) capped by Tertiary basalt (black).

112.8 km (70.1 mi) Descending into Rock Valley. Little Skull Mountain to the NW (ahead).

124.1 km (77.1 mi) Top of pass between Skull Mountain and Little Skull Mountain. Descend onto Jackass Flat.

125.8 km (78.2 mi) In the foreground to the WNW (ahead, left) is Yucca Mountain. Behind Yucca Mountain is Bare Mountain at the Skyline. To the NW (ahead) is Shoshone Mountain. The southern end of Shoshone Mountain is called the Calico Hills, the bright colors of which are due to hydrothermal alteration.

131.0 km (81.4 mi) Stop and pass through guard post and immediately turn west (left) onto Road B.

133.5 km (83.0 mi) Intersection. Turn north (right) onto 2nd Street.

137.4 km (85.4 mi) Intersection. Turn west (left) onto Forty Mile Wash Road.

139.8 km (86.9 mi) To west (ahead) is Fran Ridge in the foreground and behind it, Yucca Mountain at the skyline. To the SW (ahead left) is Busted Butte. To the north (right) are the Calico Hills.

147.4 km (91.6 mi) Begin descent into Forty Mile Wash, which is cut into the Fran Ridge and Calico Hills alluvial fans. Continue on paved road.

150.9 km (93.8 mi) Road cuts through the north end of Fran Ridge.

154.3 km (95.9 mi) Sub-dock for storage of drill pipe is on left.

154.9 km (96.3 mi) Intersection. Bear left, stay on paved road.

155.3 km (96.5 mi) Pavement ends. Continue west on dirt road which ends on drill pad for drill hole USW G-4.

155.8 km (96.8 mi) Park and walk to crest of Live and Dead Yucca Ridges to pavements 100, 200, and 300.

STOP 1. Lecture and demonstration of methods for mapping and characterizing fracture networks exposed on subhorizontal pavement surfaces.

Leave drill pad and retrace route to the sub-dock.

157.0 km (97.6 mi) Sub-dock to the west (right)

160.4 km (99.7 mi) Road cuts through north end of Fran Ridge. Continue and descend onto bottom of Forty Mile Wash.

163.2 km (101.4 mi) Turn west (right) onto dirt road and proceed up switchback to the top of Forty Mile Wash alluvial fan surface.

164.1 km (102.0 mi) Busted Butte to south (ahead). Fran Ridge to the west (right).

166.2 km (103.3 mi) Pull over onto the west shoulder of the road and park. Walk 0.40 km west up to the bottom of the saddle at the southern end of Fran Ridge and then north along ridge crest to pavement 1000.

STOP 2. Study the fracture-trace network and characteristics of fractures in the Topopah Spring Member of the Paintbrush Tuff.

Return to vehicle and continue south on dirt road around south end of Fran Ridge. Follow road to the top of Yucca Mountain.

174.9 km (108.7 mi) Intersection at top of Yucca Mountain. Pull off road and park on drill pad for drill hole USW UZ-6.

STOP 3.

Walk up to Yucca Mountain Crest to view 360-degree panorama. To the west from the skyline to Yucca Mountain crest we see, in succession, the Sierra Nevada Mountains, Panamint Range, Grapevine Mountains, Bare Mountain, Crater Flat, and Solitario Canyon. To the southeast from the skyline to Yucca Mountain crest we see, in succession, the Spring Mountains, Spector Range, Little Skull Mountain, Jackass Flat, Forty Mile Wash, and Busted Butte. To the east we see, in succession from background to foreground, the Sheep Range at the skyline, Skull Mountain, Jackass Flat, Forty Mile Wash, and Fran Ridge. To the NE we see, in succession from background to foreground, Piute Mesa at the skyline, Shoshone Range, Calico Hills, Jackass Flat, Forty Mile Wash, and Fran Ridge.

Return to vehicle and retrace route back to entrance to Nevada Test Site.

239.6 km (148.9 mi) Stop and proceed out through entrance to the Nevada Test Site. Stop to retrieve cameras and binoculars from Badge Office. Proceed south on Mercury Highway.

245.1 km (152.3 mi) Intersection. Exit onto Rte. 95 east and retrace route to Las Vegas.

270 km (167.8 mi) Cactus Springs, Nevada.

274.2 km (170.4 mi) Indian Springs, Nevada.

296.7 km (184.4 mi) Intersection with Rte. 156. Continue east on Rte. 95.

300 km (186.4 mi) To the northeast (ahead left) the dark patches on the alluvial fan derived from the Sheep Range are clumps of vegetation fed by ground-water seeps emerging from the south end of the Sheep Range. The water might be forced to the surface because the Las Vegas shear zone is an impermeable barrier to southward ground-water flow.

318.6 km (198.0 mi) Intersection. Turn south on Rte. 157 and retrace route to Mt. Charleston Hotel.

345.8 km (214.9 mi) Turn east (left) into parking area for the Mt. Charleston Hotel. End of road log. End of field trip! Banquet this evening.

REFERENCES

Andersson, Johan, and Dverstorp, Bjorn, 1987, Conditional simulation of fluid flow in three-dimensional networks of discrete fractures: Water Resources Research, v. 23, no. 10, p. 1876-1886.

Angelier, Jacques, 1984, Tectonic analysis of fault slip data sets: Journal of Geophysical Research, v. 89, no. B7, p. 5835-5848.

Anonymous, 1976, Geologic Map of the Grand Canyon National Park, Arizona: Washington, D.C., Williams & Heintz Map Co., for the Grand Canyon Natural History Association, Grand Canyon, Arizona, scale 1:62,500.

Aydin, Atilla, 1978, Small faults formed as deformation bands in sandstone: Pure and Applied Geophysics, v. 116, p. 913-930.

Aydin, Atilla and Johnson, A.M., 1978, Development of faults as zones of deformation bands and as slip surfaces in sandstone: Pure and Applied Geophysics, v. 116, p. 931-942.

Barnsley, M.F., and Demko, S., 1985, Iterated function systems and the global construction of fractals: Proceedings of the Royal Society of London, A399, p. 243-275.

Barton, C.C., 1983, Systematic jointing in the Cardium Sandstone along the Bow River, Alberta, Canada: New Haven, Conn., Yale University, Ph.D. dissertation, 301 p.

Barton, C.C., 1984, Tectonic significance of fractures in welded tuff, Yucca Mountain, southwest Nevada (abs.): Geologic Society of America, Abstracts with Programs, v. 16, no. 6, p. 438.

Barton, C.C., Gott, C.B., and Montgomery, J.R., 1986, Fractal scaling of fracture and fault maps at Yucca Mountain, southern Nevada (abs.): Eos (Transactions of the American Geophysical Union), v. 67, no. 44, p. 870.

Barton, C.C., Howard, T.M., and Larsen, Eric, 1984, Tubular structures on the faces of cooling joints--A new volcanic feature (abs.): Eos, Transactions of the American Geophysical Union, v. 65, no. 45, p. 1148.

Barton, C.C., and Larsen, Eric, 1985, Fractal geometry of two-dimensional fracture networks at Yucca Mountain, southwest Nevada, in Stephannson, Ove, ed., Fundamentals of rock joints: Proceedings of the International

155.8 km (96.8 mi) Park and walk to crest of Live and Dead Yucca Ridges to pavements 100, 200, and 300.

STOP 1. Lecture and demonstration of methods for mapping and characterizing fracture networks exposed on subhorizontal pavement surfaces.

Leave drill pad and retrace route to the sub-dock.

157.0 km (97.6 mi) Sub-dock to the west (right)

160.4 km (99.7 mi) Road cuts through north end of Fran Ridge. Continue and descend onto bottom of Forty Mile Wash.

163.2 km (101.4 mi) Turn west (right) onto dirt road and proceed up switchback to the top of Forty Mile Wash alluvial fan surface.

164.1 km (102.0 mi) Busted Butte to south (ahead). Fran Ridge to the west (right).

166.2 km (103.3 mi) Pull over onto the west shoulder of the road and park. Walk 0.40 km west up to the bottom of the saddle at the southern end of Fran Ridge and then north along ridge crest to pavement 1000.

STOP 2. Study the fracture-trace network and characteristics of fractures in the Topopah Spring Member of the Paintbrush Tuff.

Return to vehicle and continue south on dirt road around south end of Fran Ridge. Follow road to the top of Yucca Mountain.

174.9 km (108.7 mi) Intersection at top of Yucca Mountain. Pull off road and park on drill pad for drill hole USW UZ-6.

STOP 3.

Walk up to Yucca Mountain Crest to view 360-degree panorama. To the west from the skyline to Yucca Mountain crest we see, in succession, the Sierra Nevada Mountains, Panamint Range, Grapevine Mountains, Bare Mountain, Crater Flat, and Solitario Canyon. To the southeast from the skyline to Yucca Mountain crest we see, in succession, the Spring Mountains, Spector Range, Little Skull Mountain, Jackass Flat, Forty Mile Wash, and Busted Butte. To the east we see, in succession from background to foreground, the Sheep Range at the skyline, Skull Mountain, Jackass Flat, Forty Mile Wash, and Fran Ridge. To the NE we see, in succession from background to foreground, Piute Mesa at the skyline, Shoshone Range, Calico Hills, Jackass Flat, Forty Mile Wash, and Fran Ridge.

Return to vehicle and retrace route back to entrance to Nevada Test Site.

239.6 km (148.9 mi) Stop and proceed out through entrance to the Nevada Test Site. Stop to retrieve cameras and binoculars from Badge Office. Proceed south on Mercury Highway.

245.1 km (152.3 mi) Intersection. Exit onto Rte. 95 east and retrace route to Las Vegas.

270 km (167.8 mi) Cactus Springs, Nevada.

274.2 km (170.4 mi) Indian Springs, Nevada.

296.7 km (184.4 mi) Intersection with Rte. 156. Continue east on Rte. 95.

300 km (186.4 mi) To the northeast (ahead left) the dark patches on the alluvial fan derived from the Sheep Range are clumps of vegetation fed by ground-water seeps emerging from the south end of the Sheep Range. The water might be forced to the surface because the Las Vegas shear zone is an impermeable barrier to southward ground-water flow.

318.6 km (198.0 mi) Intersection. Turn south on Rte. 157 and retrace route to Mt. Charleston Hotel.

345.8 km (214.9 mi) Turn east (left) into parking area for the Mt. Charleston Hotel. End of road log. End of field trip! Banquet this evening.

REFERENCES

Andersson, Johan, and Dverstorp, Bjorn, 1987, Conditional simulation of fluid flow in three-dimensional networks of discrete fractures: Water Resources Research, v. 23, no. 10, p. 1876-1886.

Angelier, Jacques, 1984, Tectonic analysis of fault slip data sets: Journal of Geophysical Research, v. 89, no. B7, p. 5835-5848.

Anonymous, 1976, Geologic Map of the Grand Canyon National Park, Arizona: Washington, D.C., Williams & Heintz Map Co., for the Grand Canyon Natural History Association, Grand Canyon, Arizona, scale 1:62,500.

Aydin, Atilla, 1978, Small faults formed as deformation bands in sandstone: Pure and Applied Geophysics, v. 116, p. 913-930.

Aydin, Atilla and Johnson, A.M., 1978, Development of faults as zones of deformation bands and as slip surfaces in sandstone: Pure and Applied Geophysics, v. 116, p. 931-942.

Barnsley, M.F., and Demko, S., 1985, Iterated function systems and the global construction of fractals: Proceedings of the Royal Society of London, A399, p. 243-275.

Barton, C.C., 1983, Systematic jointing in the Cardium Sandstone along the Bow River, Alberta, Canada: New Haven, Conn., Yale University, Ph.D. dissertation, 301 p.

Barton, C.C., 1984, Tectonic significance of fractures in welded tuff, Yucca Mountain, southwest Nevada (abs.): Geologic Society of America, Abstracts with Programs, v. 16, no. 6, p. 438.

Barton, C.C., Gott, C.B., and Montgomery, J.R., 1986, Fractal scaling of fracture and fault maps at Yucca Mountain, southern Nevada (abs.): Eos (Transactions of the American Geophysical Union), v. 67, no. 44, p. 870.

Barton, C.C., Howard, T.M., and Larsen, Eric, 1984, Tubular structures on the faces of cooling joints--A new volcanic feature (abs.): Eos, Transactions of the American Geophysical Union, v. 65, no. 45, p. 1148.

Barton, C.C., and Larsen, Eric, 1985, Fractal geometry of two-dimensional fracture networks at Yucca Mountain, southwest Nevada, in Stephannson, Ove, ed., Fundamentals of rock joints: Proceedings of the International

Symposium on Fundamentals of Rock Joints, Bjorkliden, Sweden, p. 77-84.
Barton, C.C., Larsen, Eric, and Baechle, P.E., 1985, Fractal geometry of two-dimensional sections through fracture networks at Yucca Mountain, southwestern Nevada (abs.): Eos, Transactions of the American Geophysical Union, v. 66, no. 46, p. 1089.
Barton, C.C., Page, W.R., and Larsen, Eric, 1986, Pattern of development of fracture networks (abs.): Geologic Society of America, Abstracts with Programs, v. 18, no. 6, p. 536.
Barton, N.R., and Choubey, Vishnu, 1977, The shear strength of rock joints in theory and practice: Rock Mechanics, v. 10, p. 1-54.
Bear, Jacob, 1972, Dynamics of Fluids in Porous Media: American Elsevier, New York, 764 p.
Bohannon, R.G., 1983, Geologic map, tectonic map and structure sections of the Muddy and northern Black Mountains, Clark County, Nevada: U.S. Geological Survey Miscellaneous Investigations Series Map I-1406, scale 1:62,500.
Breed, W.J., 1975, Geological cross section of Cedar Breaks-Zion-Grand Canyon region: Springdale, Utah, Zion Natural History Association, Zion National Park, scale 1: 428,000.
Brown, S.R., and Scholz, C.H., 1985, Closure of random elastic surfaces in contact: Journal of Geophysical Research, v. 90, no. B7, p. 5531-5545.
Byers, F.M., Jr., Carr, W.J., Orkild, P.P., Quinlivan, W.D., and Sargent, K.A., 1976, Volcanic suites and related cauldrons of Timber Mountain-Oasis Valley caldera complex, southern Nevada: U.S. Geological Survey Professional Paper 919, 70 p.
Carlos, B.A., 1985, Minerals in fractures in the unsaturated zone from drill core USW G-4, Yucca Mountain, Nye County, Nevada: Los Alamos National Laboratory Report LA-10415-MS, 55 p.
Cook, N.G.W., in press, Natural joints in rock: Mechanical, hydraulic and seismic behavior and properties under normal stress: Jaeger Memorial Lecture, 29th U.S. Symposium on Rock Mechanics, 1988, 75 ms p.
Cordova, R.M., 1981, Ground-water conditions in the upper Virgin River and Kanab Creek basins area, Utah, with emphasis on the Navajo Sandstone: Utah Department of Natural Resources, Technical Publication No. 70, 87 p.
Eakin, T.E., 1966, A regional interbasin groundwater system in the White River area, southeastern Nevada: Water Resources Research, v. 2, no. 2, p. 251-271.
Eakin, T.E., and Moore, D.D., 1964, Uniformity of discharge of Muddy River Springs: U.S. Geological Survey Professional Paper 501-D, p. D171-D176.
Farmer, I.W., Daemen, J.J.K., Desai, C.S., Glass, C.E., and Neuman, S.P., eds., 1987, Rock Mechanics: Proceedings of the 28th U.S. Symposium, A.A. Balkena, Boston, Mass., 1240 p.
Gale, J.E., 1975, A numerical field and laboratory study of flow in rocks with deformable fractures: University of California at Berkeley, Ph.D. dissertation, 268 p.
Gale, J.E., Rouleau, A., and Atkinson, L.C., 1985, Hydraulic properties of fractures, in Hydrology of rocks of low permeability: Memoirs of the 17th International Congress of the International Association of Hydrogeologists, Tucson, Arizona, v. 17, part 1, p. 1-9.
Gates, H.S., 1965, Ground water in the Navajo Sandstone at the east entrance of Zion National Park, in Utah Geological Society and Intermountain Association of Petroleum Geologists, Guidebook to the Geology of Utah Number 19, Geology of south-central Utah, Salt Lake City, p. 151-160.
Goodman, R.E., and Shi, G.H., 1985, Block theory and its application to rock engineering: Englewood, N.J., Prentice-Hall, 388 p.
Gregory, H.E., 1950, Geology and geography of the Zion Park region, Utah and Arizona: U.S. Geological Survey Professional Paper 220, 200 p.
Haimson, B.C., Lacomb, J., Jones, A.H., and Green, S.J., 1974, Deep stress measurement in tuff at the Nevada Test Site: Advances in Rock Mechanics, v. IIa, National Academy of Sciences, Washington D.C., p. 557-561.
Hamilton, Warren, 1987, Plate-tectonic evolution of the western U.S.A.: Episodes, v. 10, no. 4, p.271-277.
Hamilton, Warren, 1988, Tectonic settings and variations with depth of some Cretaceous and Cenozoic structural and magmatic systems of the western United States, in W.G. Ernst, ed., Metamorphism and Crustal Evolution of the Western United States, Rubey Volume VII, Prentice Hall, Englewood Cliffs, New Jersey, p.2-40.
Hamilton, W.L., 1978, Geological map of Zion National Park: Zion Natural History Association, Springdale, Utah, scale 1:31,680.
Hamilton, W. L., 1984, The Sculpturing of Zion; Zion Natural History Association, Springdale, Utah, 132 p.
Harrill, J.R., and others, 1983, Aquifer systems in the Great Basin region of Nevada, Utah, and adjacent states: A study plan: U.S. Geological Survey Open-File Report 82-445, 50 p.
Hintze, L.F., 1980, Geologic map of Utah: Utah Geological and Mineral Survey, scale 1:500,000.
Hsieh, P.A., and Neuman, S.P., 1985, Field determination of the three-dimensional hydraulic conductivity tensor of anisotropic media--1: Theory: Water Resources Research, v. 21, no. 11, p. 1655-1665.
Hsieh, P.A., Neuman, S.P., Stiles, G. K., and Simpson, E. S., 1985, Field determination of the three-dimensional hydraulic conductivity of anisotropic media--2; Methodology and application to fractured rocks: Water Resources Research: v. 21, no. 11, p. 1667-1676.

International Association of Hydrogeologists, 1985, Hydrogeology of rocks of low permeability: International Association of Hydrologists, Memoires, v. 17, parts 1 and 2, 862 p.
King, G.C.P., 1983, The accommodation of large strains in the upper lithosphere of the earth and other solids by self-similar fault systems: The geometrical origin of b-value: Pure and Applied Geophysics, v. 121, no. 5/6, p. 761-816.
Kipp, K.L., Jr., 1987, Effect of topography on gas flow in unsaturated fractured rock: Numerical simulation, in Evans, D.D., and Nicholson, T.J., eds., Flow and Transport Through Unsaturated Fractured Rock: American Geophysical Union, Washington, D. C., p. 171-176.
Kulander, B.R., Barton, C.C., and Dean, S.L., 1979, Applications of fractography to core and outcrop investigations: U.S. Department of Energy Report METC/SP-79/3, 179 p.
Kulander, B.R., and Dean, S.L., 1985, Hackle plume geometry and joint propagation dynamics, in Stephannson, Ove, ed., Fundamentals of rock joints: Proceedings of the International Symposium on Fundamentals of Rock Joints, Bjorkliden, Sweden, p. 85-94.
La Pointe, P.R., and Hudson, J.A., 1985, Characterization and interpretation of rock mass joint patterns: Geological Society of America Special Paper 199, 37 p.
Lemos, J.V., Hart, R.D., and Cundall, P.A., 1985, A generalized distinct element program for modelling jointed rock mass, in Stephannson, Ove, ed., Fundamentals of rock joints: Proceedings of the International Symposium on Fundamentals of Rock Joints, Bjorkliden, Sweden, p. 335-343.
Long, J.C.S., 1983, Investigation of equivalent porous medium permeability in networks of discontinuous fractures: Lawrence Berkeley National Laboratory Report LBL-16259, 277 p.
Long, J.C.S., Endo, H.K., Karasaki, Kenzi, Pyrak, Laura, MacLean, Peggy, and Witherspoon, P.A., 1985, Hydrologic behavior of fracture networks, in Hydrology of rocks of low permeability: International Association of Hydrogeologists Memoirs, v. 17, part 2, Proceedings, (published by a committee of U.S.A. members of the International Association of Hydrogeologists), p. 449-462.
Maldonado, Florian, 1985, Geologic map of the Jackass Flats area, Nye County, Nevada: U.S. Geological Survey Miscellaneous Investigations Series Map I-1519, scale 1:48,000.
Maloy, K.J., Feder, Jens, and Jossang, Torstein, 1985, Viscous fingering fractals in porous media: Physical Review Letters, v. 55, p. 2688-2691.
Mandelbrot, B.B., 1982, The fractal geometry of nature: San Francisco, California, W.H. Freeman and Co., 460 p.
Maxey, G.B., and Mifflin, M.D., 1966, Occurrence and movement of ground water in carbonate rocks of Nevada, in Moore, G.W., ed., Limestone hydrology--a symposium with discussion: National Speleological Society Bulletin, v. 28, no. 3, p. 141-157.
Metcalf, L.A., 1982, Tephrostratigraphy and potassium-argon age determinations of seven volcanic ash layers in the Muddy Creek Formation of southern Nevada: Reno, University of Nevada, M.S. thesis, 187 p.
Montazer, Parviz, and Wilson, W.E., 1984, Conceptual hydrologic model of flow in the unsaturated zone, Yucca Mountain, Nevada: U.S. Geological Survey Water Resources Investigations Report 84-4345, 55 p.
Nelson, R.A., 1985, Geologic analysis of naturally fractured reservoirs: Gulf Publishing Co., Houston, Texas, 320 p.
Neuman, S.P., 1987, Stochastic continuum representation of fractured rock permeability as an alternative to the REV and fracture network concept, in Farmer, I. W., Daemen, J.J.K., Desai, C.S., Glass, C.E., and Neuman, S.P., eds., Rock Mechanics: Proceedings of the 28th U. S. Symposium: Balkema, Boston, p. 533-561.
Robinson, P.C., 1984, Connectivity, flow, and transport in network models of fractured media: Oxford, England, Oxford University, Ph.D. dissertation, 154 p.
Rogers, A.M., Harmsen, S.C., Carr, W.J., and Spence, William, 1983, Southern Great Basin seismological data report for 1981 and preliminary data analysis: U.S. Geological Survey Open-File Report 83-669, 243 p.
Scott, R.B., and Bonk, Jerry, 1984, Preliminary geologic map of Yucca Mountain, Nye County, Nevada, with geologic sections: U.S. Geological Survey Open-File Report 84-491, scale 1:12,000.
Scott, R.B., and Castellanos, Mayra, 1984, Stratigraphy and structural relations of volcanic rocks in drill holes USW GU-3 and USW G-3, Yucca Mountain, Nye County, Nevada: U.S. Geological Survey Open-File Report 84-491, 127 p.
Segall, Paul, and Pollard, D.D., 1983a, Joint formation in granitic rock of the Sierra Nevada: Geological Society of America Bulletin, v. 94, p. 563-575.
Segall, Paul, and Pollard, D.D., 1983b, Nucleation and growth of strike slip faults in granite: Journal of Geophysical Research, v. 88, no. B1, p. 555-568.
Spengler, R.W., and Chornack, M.P., 1984, Stratigraphic and structural characteristics of volcanic rocks in core hole USW G-4, Yucca Mountain, Nye County, Nevada, with a section on geophysical logs by D.C. Muller and J.E. Kibler: U.S. Geological Survey Open-File Report 84-789, 77 p.
Springer, J.E., Thorpe, R.K., and McKague, H.L., 1984, Borehole elongation and its relation to tectonic stress at the Nevada Test Site: Lawrence Livermore National Laboratory Report UCRL-53528, 43 p.

Steed, D.A., 1980, Geology of the Virgin River Gorge, northwest Arizona: Brigham Young University Geology Studies, v. 27, part 3, p. 96-115, 1:39,600 scale geologic map.
Stephansson, Ove, ed., 1985, Fundamentals of rock joints: Proceedings of the International Symposium on Fundamentals of Rock Joints, Centek, Lulea, Sweden, 582 p.
Stewart, J.H., and Carlson, J.E., 1978, Geologic map of Nevada: U.S. Geological Survey, scale 1:500,000.
Stock, J.M., Healy, J.H., Hickman, S.H., and Zoback, M.D., 1985, Hydraulic fracturing stress measurements at Yucca Mountain, Nevada, and relationship to the regional stress field: Journal of Geophysical Research, v. 90, no. B10, p. 8691-8706.
Streltsova-Adams, T.D., 1987, Well hydraulics, in Chow, V.T., ed., Heterogenous aquifer formations: Advances in Hydrosciences, v. 11, p. 357-423.
Throckmorton, C.K., 1987, Photogeologic study of linear features near a potential nuclear-waste repository site at Yucca Mountain, southern Nye county, Nevada: U.S. Geological Survey Open-File Report 87-409, 54 p.
U.S. Geological Survey, 1969, Wildcat Wash SE, Nevada topographic map, scale 1:24,000.
U.S. Geological Survey, 1983, Moapa West, Nevada: topographic map, scale 1:24,000.
Van Loenen, R.E., Sable, E.G.,Blank, H.R., Jr., Turner, R.L., Kreidler, T.J., Zelten, J.E., and Cook, K.L., 1988, Mineral Resources of the Canaan Mountain and Watchman study areas, Washington and Kane Counties, Utah: U.S. Geological Survey Bulletin 1746-A, p. A-1 - A-21, 1:50,000 scale geologic map.
Weeks, E.P., 1987, Effect of topography on gas flow in unsaturated zone: Concepts and observations, in Evans, D.D., and Nicholson, T.J., eds., Flow and Transport Through Unsaturated Fractured Rock: American Geophysical Union, p. 165-170.
Wilson, E.D., Moore, R.D., Cooper, J.R., 1969, Geologic map of Arizona: U.S. Geological Survey, scale 1:500,000.
Winograd, I.J., and Thordarson, William, 1975, Hydrogeologic and hydrochemical framework, south-central Great Basin, Nevada-California, with special reference to the Nevada Test Site: U.S. Geological Survey Professional Paper 712-C, 126 p.
Zelinski, R.A., Bush, C.A., Spengler, R.W., and Szabo, B.J., 1986, Rock-water interaction in ash-flow tuffs (Yucca Mountain, Nevada, U.S.A.)--the record from uranium studies: Uranium, v. 2, p. 361-386.